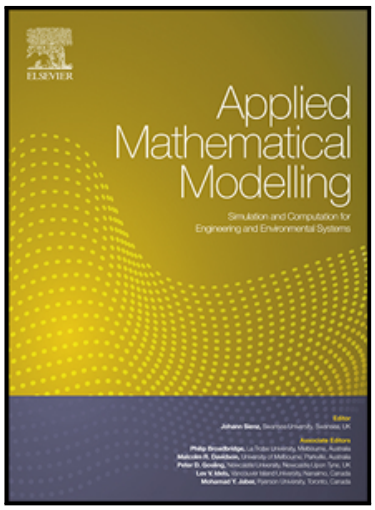

Fast spectral solutions of the double-gyre problem in a turbulent flow regime

S. Elnaz Naghibi , Sergey A. Karabasov , Mir Abbas Jalali , S.M. Hadi Sadati

PII: S0307-904X(18)30468-2
DOI: https://doi.org/10.1016/j.apm.2018.09.026
Reference: APM 12478

To appear in: *Applied Mathematical Modelling*

Received date: 22 February 2018
Revised date: 11 September 2018
Accepted date: 20 September 2018

Please cite this article as: S. Elnaz Naghibi , Sergey A. Karabasov , Mir Abbas Jalali , S.M. Hadi Sadati , Fast spectral solutions of the double-gyre problem in a turbulent flow regime, *Applied Mathematical Modelling* (2018), doi: https://doi.org/10.1016/j.apm.2018.09.026

Highlights:

- Developing a simplified model of the double-gyre problem based on layer-averaged Navier-Stokes equations
- Presenting multi-scale spectral solutions to the simplified double-gyre model
- Verification of the resulting spectral solutions with CABARET solutions of a quasi-geostrophic double-gyre model
- Validation of the spectral solutions for integral dynamic quantities and zonally averaged flow profiles

Fast spectral solutions of the double-gyre problem in a turbulent flow regime

S. Elnaz Naghibi[a, b, *], Sergey A. Karabasov[a], Mir Abbas Jalali[c], S.M.Hadi Sadati[d]

[a] School of Engineering and Materials Science, Queen Mary University of London, Mile End Road, London, E1 4NS, UK, Email: s.e.naghibi@qmul.ac.uk

[b] Department of Mechanical Engineering, Sharif University of Technology, P.O. Box: 11155-9567, Tehran, Iran

[c] Department of Mechanical Engineering, University of California, Berkeley, California 94720, USA

[d] Department of Engineering Mathematics, University of Bristol, Bristol, BS8 1TH, UK

Abstract

Several semi-analytical models are considered for a double-gyre problem in a turbulent flow regime for which a reference fully numerical eddy-resolving solution is obtained. The semi-analytical models correspond to solving the depth-averaged Navier-Stokes equations using the spectral Galerkin approach. The robustness of the linear and Smagorinsky eddy-viscosity models for turbulent diffusion approximation is investigated. To capture essential properties of the double-gyre configuration, such as the integral kinetic energy, the integral angular momentum, and the jet mean-flow distribution, an improved semi-analytical model is suggested that is inspired by the idea of scale decomposition between the jet and the surrounding flow.

Keywords: ocean modelling, double-gyre, Galerkin approximation, multi-scale

Glossary

β-plane approximation	a planar mapping of spherical-surface ocean domains based on a linear approximation of the Coriolis parameter around a reference latitude
double-gyre	a pair of counter-rotating large-scale oceanic currents
hydrostatic model	a reduction of 3D Navier-Stokes equations assuming static balance between pressure gradients and the gravity in vertical direction
oceanic general circulation models	global models of interconnected oceans in interaction with the Earth's crust and atmosphere using mass, momentum and energy conservations
geostrophic balance	a reduction of 3D Navier-Stokes equations assuming exact balance of horizontal

	pressure gradients and Coriolis terms
meso-scale eddies	10-100 Km circulating structures in oceans determining the transient behaviour of larger-scale currents
quasi-geostrophic model	a mid-latitude approximation of 3D Navier-Stokes equations based on perturbing the geostrophic equations using β-plane approximation
quasi-hydrostatic model	a perturbation of the hydrostatic model in which the balance of pressure gradients and the gravity is disturbed while vertical velocity dynamics is still negligible
potential vorticity	a quantity combining vorticity and two further terms arising from the latitudinal gradient of the Coriolis parameter and vertical buoyancy gradient

1. Introduction

Global oceans, which absorb of about 90 percent of radiation energy coming from the atmosphere, generate turbulence with a sheer diversity of flow scales which range from meter-size internal waves to meso-scale currents with the characteristic size of hundreds of kilometres [1]. In the literature, the ocean dynamics has been simulated from most complex comprehensive models to idealised systems.

At the most comprehensive level, prognostic equations for velocity, density and salinity are solved with appropriate boundary conditions such as a realistic coastline geometry, the ocean bottom topography, as well as the local atmospheric temperature and wind effects as informed by observations. Starting from the work of Marshall [2], who extended the hydrostatic ocean model to quasi-hydrostatic and non-hydrostatic models, there have been several developments in the direction of increasing the fidelity of ocean dynamics simulations. Most notably, these developments include general circulation ocean dynamics models POP [3], NEMO [4], and MITgcm [5], as well as specialised, regional ocean models such as ROMS by Shchepetkin and McWilliams [6]. Most advanced of these models operate with terrain-fitted coordinates and use high-order finite-volume or finite-elements methods for solving the governing Navier-Stokes equations [7]. In other works, such as in [8], complex ocean effects including continuity, momentum, thermodynamics, and salinity transport are investigated using dynamical system analysis tools.

In comparison with the comprehensive ocean models, the idealised ocean models focus on a certain aspect of ocean dynamics, thus, allowing to significantly reduce the physical and geometrical complexity. For example, Munk developed an ocean dynamics model based on quasi-geostrophic potential vorticity equations to study wind-driven ocean circulations for zonal, meridional and circular winds [9]. The models of this type are particularly useful for the investigation of meso-scale dynamic mechanisms behind wind-driven ocean systems. One

example of such systems is the North Atlantic subtropical gyre, which together with its smaller subpolar counterpart constitute a double-gyre system that is well-known for its eastward jet extension, Gulf Stream. Another example is subpolar and subtropical gyres and the meandering eastward jet, Kuroshio that constitute a double gyre system in the North Pacific. To elucidate the role of meso-scale eddies in double gyre systems, Holland considered a simplified configuration of the two-layer quasi-geostrophic model in [10]. However, even in this simplified configuration, for the high Reynolds numbers of interest, the dynamics of double gyre systems contains a broad range of scales which require a significant numerical grid resolution to simulate accurately. To investigate the role of meso-scale oceanic eddies within the double-gyre system and develop a model for the fine-scales in a turbulent, eddy-resolving regime Berloff [11] decomposed a high-resolution flow solution into large-scale and the 'turbulent oscillator' represented by small-scale eddy components. Further works by Karabasov, Berloff and Goloviznin [12] and also by Shevchenko and Berloff [13] continued to investigate dynamics and energy balances of the double-gyre system at small viscosity regimes by using advanced high-resolutions numerical methods such as the CABARET scheme as well as refined numerical grids. Along a similar line of research, Maddison et al. [14] used refined numerical grids to investigate the effect of potential vorticity fluxes on the dynamics of the double-gyre system by decomposing eddy potential vorticity fluxes into divergent and rotational components. Another example of high-fidelity simulations for the double-gyre problem can be found in [15] which applied high-order spectral elements for numerical accuracy.

A large emphasis on purely numerical solutions of the double gyre problem in turbulent, eddy-resolving regimes in the above studies can be related to the analysis by Berloff [11]. Among other things, the later work showed that because of the complexity of the double-gyre system, the effect of the small eddies, which are a key element of the jet development, cannot be reproduced by conventional turbulent diffusion parameterisations such as the standard Smagorinsky eddy-viscosity model [16]. That is, the standard fine-scale closure models for Reynolds stress based on diffusion, which allow one to essentially simplify the governing partial differential equations and thus to obtain a semi-analytical model, cannot represent characteristic features of the double gyre such as the jet flow. Consistently with these findings, despite a significant effort devoted to development of semi-analytical solutions of Navier-Stokes solutions, little has been achieved in developing such solutions for ocean dynamics problems in turbulent flow regimes. A brief overview of analytical model developments relevant to the purpose of the current discussion is presented below.

Semi-analytical solutions of Navier-Stokes equations include the use of the Petrov-Galerkin method [17, 18], the Taylor series expansion method [19], the integral transforms [20] and the Homotopy perturbation method [21, 22]. Furthermore, in [23-25], WKB perturbation technique was applied for solving Navier-Stokes equations for weakly nonlinear problems. Fengler introduced a wavelet-based Galerkin method to solve Navier-Stokes equations on rotating spheres [26]. Il'In and Filatov proved the existence and uniqueness of generalized solutions for Navier-Stokes equations using Galerkin's approximation [27]. Cao et al. proved Gevrey regularity and showed exponential convergence of spectral Galerkin method with spherical harmonic functions with application to solving the Navier-Stokes equations on the rotating two-dimensional sphere [28]. To the best knowledge of the authors, except for the recent work by Jamal [29] which uses Lie symmetries to find closed-form analytical solution to the double-gyre problem, no analytical or semi-analytical study has been devoted to solving Navier-Stokes equations using continuous spectral methods in application to modelling of wind-driven ocean dynamics in a non-linear regime such as for the double-gyre problem.

On the other hand, analytical and semi-analytical solutions to Navier-Stokes equations of the meso-scale oceanic currents such as double gyre at eddy-resolving regimes have a special importance. Such reduced-order models can not only be used for verification of comprehensive ocean dynamics models but also for conducting large-scale parametric studies. For example, reduced-order ocean models with a focus on the meso-scale ocean dynamics can be particularly useful in modelling of long-term variability due to the ocean dynamics interaction with geophysical phenomena. One of such interactions has been studied in the work by Naghibi et al. [30] who considered the effect of the oceanic currents on the Earth's pole rotation also known as the Chandler wobble effect.

The goal and the novelty of the current work is in revisiting the conclusions by Berloff [11] by developing a novel framework for semi-analytical modelling suitable for the double-gyre problem. Here we apply a multi-scale approach [31] with assuming a scale separation between the small eddies essentially contributing to the jet development and the surrounding large-scale gyres. The resulting model is closed with a conventional diffusion approximation and the entire system is efficiently solved using spectral elements, which are developed in a systematic manner. The success of the resulting semi-analytical model would prove that the complex double-gyre system, which has been attracting attention since 1950s is amenable to a relatively simple scale-separation method with a turbulent diffusion approximation applied. This success is judged by comparing the semi-analytical solution with the reference eddy-

resolving model in order to verify how well the approximate model captures key meso-scale features of the double gyre system: the zonally averaged jet mean-flow field and the integral angular momentum and kinetic energy. The current work can also be seen as an expanded analysis of the fluid dynamics model underlying the development of the ocean dynamics – Chandler wobble model in [30].

The paper is organised as the following. Section 2 describes the general Navier-Stokes equations for three-dimensional flow of incompressible fluids in a rotating frame. In Section 3, details of the governing three-layer quasi-geostrophic equations together with the boundary conditions are reviewed and its eddy-resolving computational solution is provided as a reference for the rest of the paper. In Section 4, simplified depth-averaged Navier-Stokes equations are considered which correspond to a latitude-longitude quadrangle in the rotating frame and a double-gyre wind forcing configuration. Semi-analytical solutions of these equations using a spectral Galerkin approach are obtained for linear eddy viscosity model. To account for a better parameterization of the turbulent mixing effects, a Smagorinsky eddy-viscosity model is implemented for the same model and its solution is obtained using a semi-analytical Galerkin approximation. In Section 5, the semi-analytical solutions are further extended to capture the eastward jet effect in the framework of a newly developed two-scale model and the semi-analytical solutions obtained are compared with the reference eddy-resolving solution based on the direct numerical simulation of the double-gyre problem.

2. General Navier-Stokes equations for incompressible flows in a rotating frame

The three-dimensional Navier-Stokes momentum and continuity equations for incompressible flow in a rotating frame of reference are given in vector notation by:

$$\begin{aligned} &\frac{\partial \mathbf{v}}{\partial t}+(\mathbf{v}.\nabla)\mathbf{v}+\boldsymbol{\omega}(\boldsymbol{\omega}\times\mathbf{r})+2\boldsymbol{\omega}\times\mathbf{v}=\mathbf{f}-\frac{\nabla P}{\rho}+\frac{\nabla.\boldsymbol{\tau}}{\rho}+\frac{\mathbf{T}}{h_w}, \\ &\nabla.\mathbf{v}=0, \end{aligned} \tag{1}$$

where $\mathbf{v}$ is the velocity vector, $\boldsymbol{\omega}$ is the earth's angular velocity, $\mathbf{r}$ is the ocean particle position vector, P is the hydrostatic pressure, $\mathbf{f}$ is the body force per unit mass, $\boldsymbol{\tau}$ is deviatoric stress tensor. $\mathbf{T}$ is the wind stress vector per unit density exerted on ocean surface and h_w is the ocean depth exposed to the wind forcing.

The solution of the full Navier-Stokes equations for oceanic flows, which correspond to a vast diversity of length scales from meso-scale currents (10-100 km) to internal waves (1-10 m) is extremely complex. The focus of the current modelling is meso-scale ocean turbulence,

such as the one which plays a dominant role in the Gulf Stream current dynamics, and we use three simpler models for the governing double-gyre problem: a stratified quasi-geostrophic model used as the reference (model *i*), a (single-scale) layer-averaged model with and without turbulence approximation (model *ii*), which is an intermediate model used in the development of the final low fidelity model, and eventually a two-scale layer-averaged model of the double-gyre together its eastward jet employing turbulence approximation and scale decomposition (model *iii*).

In the high-fidelity model (model *i*), which is based on the well-known quasi-geostrophic approximation, variation in the ocean depth are handled through layer stratification and the resulting two-dimensional multi-layer non-linear partial differential equations are solved numerically using a high-resolution scheme. The finally suggested low fidelity model (model *iii*) is a two-scale layer-averaged model using eddy viscosity approximation in which the two-dimensional spectral expansions transform the governing partial differential equations to ordinary differential equations in time with fast turn-around solutions. The simplifying assumptions together with the definition of the translated parameters are presented in Appendix A.

3. Model *i*: stratified quasi-geostrophic double-gyre model

3.1. Governing equations, boundary conditions and wind forcing

The quasi-geostrophic model of the wind-driven double-gyre circulation is considered in a mid-latitude closed basin, which is in the shape of a longitude-latitude quadrangle with north–south ($\phi = \text{const}$) and east–west ($\theta = \text{const}$) rigid walls. The boundaries correspond to meridians $\phi_1 = -\phi_2 = -0.4102$ radians and lines of colatitude $\theta_1 = 0.5236$ and $\theta_2 = 1.126$ radians mapped to the Cartesian region of $0 \le x, y \le L$ according to β-plane approximation. The size of the computational domain corresponds to 3840km×3840km. The model simulates North Atlantic subpolar and subtropical ocean gyres as well as the western boundary current, the Gulfstream, and its eastward jet extensions between approximate latitudes of Greenland and Canary Islands [10, 12, 13]. The governing equations constitute the system of material conservation laws for potential vorticity (PV) with a source term due to the meridional gradient of the Coriolis parameter and with the additional source terms due to the lateral viscosity, bottom friction, and the wind forcing in Cartesian coordinates (Eq. A.15):

$$\partial_t q_i + J(\psi_i, q_i) = \delta_{1i} F_w - \delta_{i3} \frac{a_v}{H_3^2} \Delta\psi_i + a_h \Delta^2 \psi_i,\ i = 1,2,3, \quad (2)$$

where F_w, a_v and a_h are wind curl forcing, bottom friction and lateral viscosity coefficients, respectively. δ_{ij} is the Kronecker symbol, ψ_i is quasi-geostrophic stream function, q_i is the quasi-geostrophic potential vorticity and $J(f,g) = f_x g_y - f_y g_x$. The three horizontal isopycnal (constant density) layers are dynamically coupled through pressure fluctuations (Eq. A.16) so that

$$q_i = \nabla^2 \psi_i + \beta y - (1-\delta_{i1}) S_{i1} (\psi_i - \psi_{i-1}) - (1-\delta_{i3}) S_{i2} (\psi_i - \psi_{i+1}), i = 1,2,3, \quad (3)$$

where $\beta = 2\times10^{-11}\,\mathrm{m^{-1}s^{-1}}$ is the Coriolis parameter gradient and the stratification parameters S_{i1} and S_{i2} are selected so that the first and second Rossby deformation radii are $Rd_1 = 40$ km and $Rd_2 = 23$ km, respectively. Rossby radii of deformation, depending on latitudinal range of the ocean domain and density ratio of the layers, are inverse square root of the stratification matrix eigen values, (see Eq. A.17-26). The depths of layers are $H_1 = 250$, $H_2 = 750$ and $H_3 = 3000$ meters numbered from the top. On the lateral walls, partial-slip boundary conditions are applied

$$\partial_{\mathbf{nn}} \psi_i - \alpha^{-1} \partial_{\mathbf{n}} \psi_i = 0, i = 1,2,3, \quad (4)$$

so that the slip length α is equal to 120 km and $\mathbf{n}$ is the unit vector normal to the boundaries.

Following Shevchenko and Berloff [13], the following steady wind forcing function is used

$$F_w = \begin{cases} A\sin\left(\frac{\pi y/L}{y_0/L}\right) & 0 \le y < y_0 \\ -B\sin\left(\frac{\pi(y-y_0)/L}{1-y_0/L}\right) & y_0 \le y \le L \end{cases} \quad (5)$$

where

$$A = -\frac{2\pi\sigma \times W_{asym}}{H_1},\ B = \frac{2\pi\sigma}{W_{asym} \times H_1},\ y_0 / L = 0.5 + W_{tilt} \times (x/L - 0.5), \quad (6)$$

and $W_{asym} = 0.9$ and $W_{tilt} = 0.2$ are taken for the wind asymmetry and tilt parameters, respectively. The wind curl amplitude is assumed to be $\sigma = 8\times10^{-5}\,\frac{\mathrm{m}^2}{\mathrm{s}^2}$ and lateral viscosity and bottom friction coefficients are taken to be $a_h = 100\,\frac{\mathrm{m}^2}{\mathrm{s}}$ and $a_v = 0.36\,\frac{\mathrm{m}^2}{\mathrm{s}}$, respectively,

which correspond to a turbulent flow regime [13]. In Appendix A, the derivation details of the stratified quasi-geostrophic equations (Eq. (2)) from the three-dimensional Navier-Stokes equations (Eq. (1)) are provided.

3.2. Eddy resolved solutions

A solution of the above boundary value problem is obtained by solving it numerically using the high-resolution CABARET method of Karabasov and Goloviznin on a uniform Cartesian grid of 512^2 cells [32]. Following Karabasov and Goloviznin [32], the numerical solution is started from zero initial conditions, run for a spin out time of 8000 days until it reaches statistical stationarity (to guarantee that the result of ensemble averaging no longer depends on the starting time of the time averaging) and then left running for a long enough simulation time (3650 days) for the solution to converge statistically. One simulation of the eddy-resolving double-gyre model typically takes about 34 hours on four IBM System X iDataPlex dx360 M3 Server nodes (2 × 6-Core 2.4 GHz Intel Xeon E5645 (Westmere) CPU and 24 GB RAM) in Queen Mary HPC cluster, Apocrita [33]. The eddy-resolving solution obtained is used for calibration of the semi-analytical models *ii* and *iii*.

Fig. 1a and b show typical snapshots of instantaneous distributions of potential vorticity and its fluctuations from the time-averaged state, respectively. Both solutions are shown for the top layer where the eastward jet is most pronounced. The jet, being one of the most important features of this flow, separates from the west boundary under the wind forcing effect which spins the flow into the two counter-rotating gyres. The jet is distinguished from the large-scale surrounding flow by a narrow region of high-amplitude fast-evolving coherent structures which propagate from west to east. The characteristic features of the jet will be used for the semi-analytical two-scale model of the double-gyre problem to be discussed in section 5.

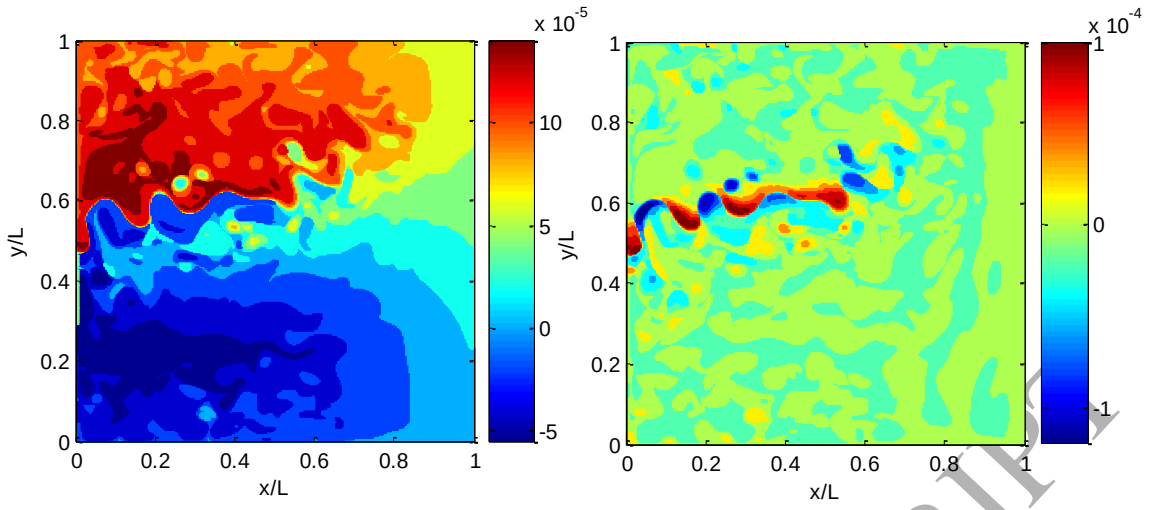

(a) (b)

Fig. 1. Instantaneous flow solutions of the double-gyre problem in an eddy resolving regime for the top isopycnal layer: PV (a) and PV fluctuation (b).

4. Model *ii*: A simplified double-gyre model based on depth-averaged Navier-Stokes equations

4.1. Governing equations, boundary conditions and turbulence closure

To present a simplified depth-averaged double-gyre model, we take the curl of Eq. (1), to eliminate pressure gradients, centrifugal terms, and conservative body forces:

$$\frac{\partial \boldsymbol{\zeta}}{\partial t} + (\mathbf{v}.\nabla)\boldsymbol{\zeta} = \nabla \times \left(\frac{\nabla.\boldsymbol{\tau}}{\rho} + \frac{\mathbf{T}}{h_w} \right) + (\boldsymbol{\zeta}.\nabla)\mathbf{v} + 2(\boldsymbol{\omega}.\nabla)\mathbf{v}, \qquad (7)$$

where $\boldsymbol{\zeta}$ is the vorticity vector. Then we use spherical coordinates, (r,θ,ϕ), where r is the radial distance from the centre of the Earth, and θ and ϕ are co-latitudinal and azimuthal angles, respectively. We integrate Eq. 7 along the radial direction to find the depth-averaged transport equation for mean vorticity. We work with the radial component of the above relation which corresponds to the normal vorticity component, $\zeta^{\perp} = \frac{1}{r\sin\theta}\left(\frac{\partial}{\partial\theta}(\sin\theta v_{\phi}) - \frac{\partial v_{\theta}}{\partial\phi} \right)$. The resulting equation in spherical coordinates (curl of Eq. (B.1), Appendix B) including the lateral and vertical (bottom) friction terms will be fully analogous to the depth-averaged equation (Eq. (A.31)) in the Cartesian coordinates, which was derived in Appendix A for mean vorticity transport in beta plane.

For the depth-averaged model, full slip conditions are imposed along the zonal and meridional boundaries so that

$$v_\theta(\theta_1,\phi,t)=v_\theta(\theta_2,\phi,t)=v_\phi(\theta,\phi_1,t)=v_\phi(\theta,\phi_2,t)=0. \quad (8)$$

For the solution, the Eq. 7 is supplemented with the continuity equation relating the meridional and the zonal velocity components which under the assumption of zero radial velocity is

$$\frac{v_\theta\cot\theta}{r}+\frac{1}{r}\frac{\partial v_\theta}{\partial\theta}+\frac{1}{r\sin\theta}\frac{\partial v_\phi}{\partial\phi}=0. \quad (9)$$

For the non-linear flow regime which corresponds to small viscosity values of a_h and a_v, the spectral solution of the above model cannot resolve the turbulent mixing phenomena and fails to converge.

In an attempt to explicitly model the turbulent mixing, the Smagorinsky non-linear eddy-viscosity model is considered next to extend the validity of the proposed model to high Reynolds numbers. For modelling of non-linear eddy-viscosity effects, the standard procedure [34] of decomposing the flow solution into the ensemble averaged ("filtered") solution and the fluctuation, $\mathbf{v}=\bar{\mathbf{v}}+\mathbf{v}'$, substituting the decomposition into the governing Eq. (1), and ensemble averaging the result is applied.

This leads to a system of equations with regard to the ensemble averaged solution component which is not closed because of the quadratic non-linearity of the Navier-Stokes equations, $(\mathbf{v}.\nabla)\mathbf{v}$,

$$\overline{(\mathbf{v}.\nabla)\mathbf{v}}-(\bar{\mathbf{v}}.\nabla)\bar{\mathbf{v}}=(\nabla.\bar{\tau})^{\text{turbulence}}. \quad (10)$$

In the framework of the Smagorinsky model [16], the corresponding non-linear stress term on the right-hand side is approximated by an ensemble averaged strain rate tensor with an effective turbulent viscosity function ν dependent on strain rate magnitude

$$\bar{\tau}_{ij}=\rho\overline{v_i'v_j'}=\nu(|\mathbf{S}|)\bar{S}_{ij}. \quad (11)$$

In the model, the vertical and horizontal eddy viscosity functions (ν_{Tv} and ν_{Th}) are proportional to the rate of deformation tensor so that

$$\nu_{Tv} = (C_s\Delta)^2 \left|\bar{S}_v\right| = (C_s\Delta)^2 \sqrt{2\left(2\bar{S}_{12}\bar{S}_{12} + 2\bar{S}_{13}\bar{S}_{13}\right)},$$
$$\nu_{Th} = (C_s\Delta)^2 \left|\bar{S}_h\right| = (C_s\Delta)^2 \sqrt{2\left(\bar{S}_{22}\bar{S}_{22} + 2\bar{S}_{23}\bar{S}_{23} + \bar{S}_{33}\bar{S}_{33}\right)}, \tag{12}$$

where C_s is a calibration parameter of the Smagorinsky model, S_{ij} is the rate of deformation tensor, and $\bar{S}_{ij}$ is its time average. Δ is the length scale such that

$$\Delta = \sqrt[3]{\frac{\pi^2 H}{k_\phi k_\theta}}, \tag{13}$$

and k_θ and k_ϕ are the cut-off wave numbers in meridional and zonal spectral expansions.

4.2. Solution method

To solve the normal component of Eq. (7), the Fourier-Galerkin spectral method [35] is applied. The method is based on considering the basis functions for velocity components that have time varying amplitudes and satisfy full slip boundary conditions. For the zonal velocity component, the following form is assumed:

$$v_\theta = \sum_{m=1}^{M}\sum_{n=1}^{N} Y_{mn}(t)\sin\left[m\omega_\theta(\theta-\theta_1)\right]\cos\left[(2n-1)\omega_\phi(\phi-\phi_1)\right], \tag{14}$$

where

$$\omega_\theta = \frac{2\pi}{\theta_2-\theta_1},\ \omega_\phi = \frac{\pi}{\phi_2-\phi_1}, \tag{15}$$

and the meridional velocity component is obtained from the continuity Eq. (9) so that

$$v_\phi = -\sum_{m=1}^{M}\sum_{n=1}^{N} \frac{Y_{mn}(t)}{(2n-1)\omega_\phi}\sin\left[(2n-1)\omega_\phi(\phi-\phi_1)\right]$$
$$\times\left\{\cos\theta\sin\left[m\omega_\theta(\theta-\theta_1)\right] + m\omega_\theta\sin\theta\cos\left[m\omega_\theta(\theta-\theta_1)\right]\right\}. \tag{16}$$

Next, the weak solution is obtained by applying the Galerkin formulation through multiplying the vorticity basis functions by both sides of normal component of Eq. (7) after substituting velocity components from Eqs. (14) and (16)

$$w_{ij}\cdot\left[\sum_{m=1}^{M}\sum_{n=1}^{N}\dot{Y}_{mn}(t)a_{mn} + \sum_{m=1}^{M}\sum_{n=1}^{N}Y_{mn}(t)b_{mn} + \sum_{m=1}^{M}\sum_{n=1}^{N}\left(\sum_{\mu=1}^{M}\sum_{\nu=1}^{N}Y_{\mu\nu}(t)c_{\mu\nu}\right)Y_{mn}(t)d_{mn}\right] =$$
$$\sum_{m=1}^{M}\sum_{n=1}^{N}\dot{Y}_{mn}(t)\left[w_{ij}.a_{mn}\right] + \sum_{m=1}^{M}\sum_{n=1}^{N}Y_{mn}(t)\left[w_{ij}.b_{mn}\right] + \sum_{m=1}^{M}\sum_{n=1}^{N}\sum_{\mu=1}^{M}\sum_{\nu=1}^{N}Y_{\mu\nu}(t)Y_{mn}(t)\left[w_{ij}.(c_{\mu\nu}d_{mn})\right] = 0, \tag{17}$$

in which a_{mn} are the space dependent coefficients of time derivatives of velocity amplitudes. b_{mn} and $c_{\mu\nu}d_{mn}$ represent linear and nonlinear space-dependent coefficients of velocity amplitudes in the governing equation, respectively. w_{ij} are the vorticity basis functions obtained by combining Eqs. (14), (16), and the definition of vorticity in spherical coordinates

$$w_{ij} = \sin\left[j\omega_\phi(\phi-\phi_1)\right]\{(1+i^2\omega_\theta{}^2)\sin\left[i\omega_\theta(\theta-\theta_1)\right]\sin^2\theta + j^2\omega_\phi{}^2\sin\left[i\omega_\theta(\theta-\theta_1)\right] \\ -\sin\left[i\omega_\theta(\theta-\theta_1)\right]\cos^2\theta - 3i\omega_\theta\cos\left[i\omega_\theta(\theta-\theta_1)\right]\cos\theta\sin\theta\}/(j\omega_\phi\sin\theta), 1\le i\le M, 1\le j\le N. \quad (18)$$

Upon weighting, the resulting equations are numerically integrated over the final grid of 128×128 elements in the (ϕ,θ)-domain and a set of ordinary differential equations $\dot{\mathbf{Y}} + \mathbf{C}.\mathbf{Y} + \mathbf{N}(\mathbf{Y}) = 0$ for the unknown velocity amplitudes $Y_{mn}(t)$ is obtained, where $\mathbf{Y} = \left[Y_{11}(t) \ \ . \ . \ . \ \ Y_{MN}(t)\right]^T$. Matrix $\mathbf{C}$ represents all linear terms of the weighted equation and $\mathbf{N}(\mathbf{Y})$ stands for a nonlinear vector resulting from all the convective and turbulence terms. The resulting nonlinear ordinary differential equations are solved numerically using a fourth-order Runge-Kutta scheme with integration time step equal to 2 days. In comparison with solving the original partial differential Eq. (2), the high-accuracy solution of the ordinary differential equations takes only a small fraction of the computational cost.

4.3. Stabilizing role of Smagorinsky eddy viscosity model

Fig. 2 shows the solutions of the first velocity amplitude component as obtained with a nine-term spectral Galerkin method ($M=N=3$) with the linear eddy viscosity model (no non-linear parameterisation) and the Smagorinsky eddy viscosity parameterisation ($C_s=0.1$). A steady converged solution is only obtained for the latter case while the linear eddy viscosity model diverges for the same values of the lateral viscosity, bottom friction viscosity, and the wind forcing parameters, $a_h = 10\ \frac{\mathrm{m}^2}{\mathrm{s}}, a_v = 0.036\ \frac{\mathrm{m}^2}{\mathrm{s}}, \sigma = 8\times10^{-5}\ \frac{\mathrm{m}^2}{\mathrm{s}^2}$. The lateral viscosity value corresponds to Reynolds number $\mathrm{Re} = UL a_h^{-1}$ of about 16000 based on the basin size $L = 3840\,\mathrm{Km}$ and $U = \tau_0\left(\rho_1 H_1 L\beta\right)^{-1} = 0.0417\,\mathrm{m/s}$. Notably, the spectral solution based on the linear eddy viscosity model keeps diverging even for increasingly high values of Reynolds number.

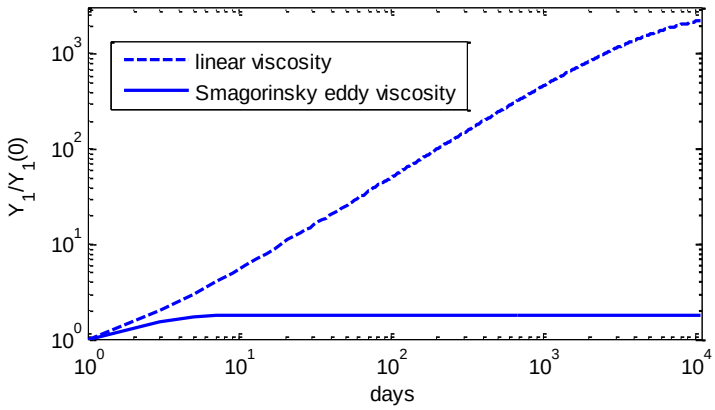

Fig. 2. The stabilising role of the non-linear eddy-viscosity model: first-term velocity amplitude for the spectral solution. Dotted lines represent solutions of the linear eddy viscosity model and solid line stand for the solutions of the Smagorinsky model.

By replacing the linear eddy viscosity model with the Smagorinsky turbulent diffusion parameterisation, it is possible to obtain a steady converged solution for the depth-averaged Navier-Stokes equations. Moreover, by tuning the model calibration parameter C_s it is even possible to obtain the same integral characteristics such as integral angular momentum of the system as compared with the reference eddy-resolved solution. However, a simultaneous preservation of both the integral angular momentum and the integral kinetic energy by the simplified depth-averaged model (Eq. 7) is not possible through tuning the model parameters, such as the Smagorinsky constant or the lateral and bottom friction viscosity coefficients. Moreover, regardless of the choice of the calibration parameters, the simplified model does not contain the most important feature of the double-gyre problem – the jet flow (Fig. 1). This is consistent with Berloff [11] who argued that the eddy dynamics of the double-gyre problem in a turbulent flow regime cannot be represented by a parameterisation based on the turbulent diffusion. Hence, a better semi-analytical model which takes into account the jet feature of the double-gyre problem is developed in the next section based on the idea of scale separation.

5. Model *iii*: A two-scale model for the double-gyre problem

5.1. Model development: two-scale governing equations and boundary conditions

The jet is a distinct feature of the double-gyre problem. As discussed in section 3, it is characterised by the flow of coherent vertical structures in a narrow region between the two

counter-rotating gyres which contain much less coherent vortices quickly mixing out in the surrounding regions close to the walls of the solution domain. In comparison with the flow in the latter regions, the jet generally corresponds to higher velocity amplitudes and smaller flow scales in the direction normal to the jet flow. Thus, a modification of the depth-averaged Navier-Stokes model from the previous section is suggested to provide a better approximation of the double-gyre flow by exploiting the scale separation between the jet and the surrounding flow.

Let's consider a two-scale model which is based on decomposing all flow variables into two scales in space and time. For example, the velocity field is decomposed so that

$$\mathbf{v} = \mathbf{v}^{(l)} + \mathbf{v}^{(L)}, \qquad \frac{l}{L} = \frac{\tau}{T} << 1, \qquad \frac{\left|\mathbf{v}^{(L)}\right|}{\left|\mathbf{v}^{(l)}\right|} << 1, \tag{19}$$

where $\mathbf{v}^l$ and $\mathbf{v}^L$ are the jet and gyre scale velocity components, which correspond to the jet and the gyre time and space length scales, τ, T and l, L, respectively.

Furthermore, we will assume that the jet-scale solution, $\mathbf{v}^l$ is nonzero in a narrow strip stretched in the longitudinal direction with two latitude lines, $\theta = \theta_1'$ and $\theta = \theta_2'$ ($\theta_1 < \theta_1', \theta_2' < \theta_2$) as the top and the bottom boundaries of the effective jet location, respectively. The gyre-scale solution, $\mathbf{v}^L$ is defined in the entire double-gyre domain.

Because of asymmetry of the jet location that is sensitive to the asymmetry and tilt parameters of the wind forcing as well as to the viscous boundary layer effects, the precise location of the separation point of the jet at the west boundary is slightly offset from the centreline latitude. To mimic this in the semi-analytical modelling, the same latitude of the jet centreline location $(\theta_1' + \theta_2')/2$ is used as in the reference eddy-resolving double-gyre solution.

Detailed derivation steps are provided in Appendix B. Briefly, through substitution of the flow decomposition Eq. (19) in Eq. (1), making the resulting equations dimensionless and re-arranging them, the jet-scale and the gyre-scale terms are grouped separately. Under the assumption of scale separation, this leads to two coupled systems of equations for the jet-scale and for the gyre-scale velocity components accordingly. Then, to facilitate the semi-analytical solution, the jet-scale and the gyre-scale sets of equations are made separable one from the other by using further appropriate approximations of the nonlinear Reynolds stress

terms. In case of the gyre-scale equation, this approximation amounts to using the Smagorinsky eddy viscosity model and for the jet-scale solution the effects due to the scales finer than the small scale (jet scale) of the two-scale model are ignored.

The physical idea behind the above scale separation method is illustrated in Fig. 3. Here, Fig. 3a shows the time and layer-averaged meridional velocity distribution obtained from the eddy-resolved numerical simulation of the reference double-gyre problem. There are three flow scales evident in this figure: small scales associated with turbulent mixing, large scales associated with coherent structures in the jet, and very large scales associated with the gyre circulations which are driven by the wind forcing that initiates the jet flow. The corresponding wavenumber spectra of kinetic energy is shown in Fig. 3b which includes the same three features: a large energy containing peak at small wavenumbers which corresponds to the gyre scale and the wind forcing, a second spectral peak at the intermediate wavenumbers which corresponds to the jet flow, and a monotonically decaying part of the high-wavenumber spectra which corresponds to turbulence dissipation and small scales.

It can be noticed that the wavenumber spectrum of the double-gyre flow at the eddy-resolving regime does not monotonically decay to directly dissipate energy of the wind-driven gyres through viscosity at the small scale but includes a second peak which corresponds to the coherent jet structures.

In order to capture all these three features, in addition to the classical turbulent diffusion model which describes the gradual dissipation of wind energy by viscous dissipation, one needs to include a separate model to represent the jet flow. This is exactly what is done in the suggested two-scale model, which approximates the original two-peak spectrum of the double-gyre flow by a combination of the two sub-spectra representing the gyre-scale and the jet-scale parts of the model. The two sub-models correspond to different scales, hence, their spectra are offset in the wavenumber space.

The gyre-scale part of the two-scale model (blue dashed line) includes Very Large Scales (VLS), which correspond to the first peak due to the wind forcing, and Small Scales (SS), which correspond to the turbulent dissipation in accordance with the Smagorinsky eddy viscosity model. Large Scales (LS) of the jet dynamics, which are responsible for the second peak in the energy spectra, are represented by the jet part of the two-scale model (red dashed line). Here the effect of the high wavenumber spectra is neglected since it decays faster than

the high wavenumber spectra of the gyre-scale part of the solution (compare red dashed line with blue dashed line).

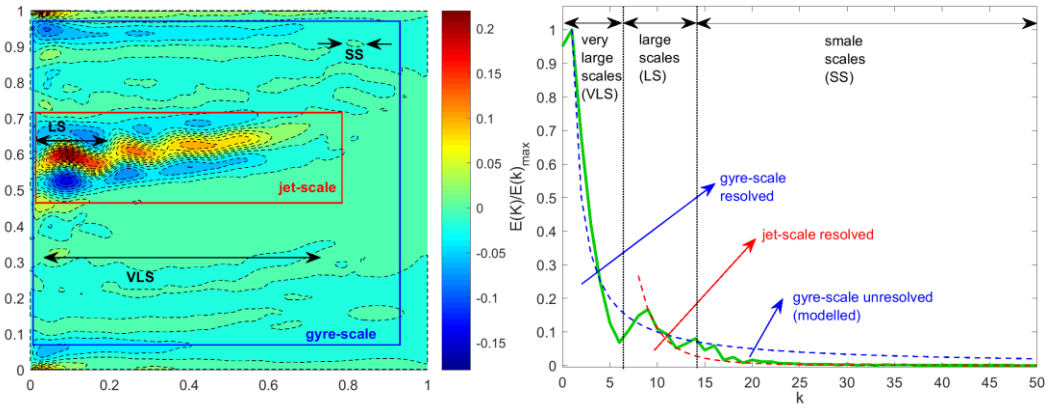

(a) (b)

Fig. 3. Physical interpretation behind the two-scale model of the double-gyre flow: time and layer-averaged meridional velocity distribution (a) and kinetic energy spectrum of the double-gyre flow in wavenumber space for equal meridional and zonal wave numbers (b). The scale decomposition idea to capture the two-peak energy spectra together with a turbulence diffusion approximation provides a reduced-order model for the double-gyre problem.

5.2. Solution method

The final result, in accordance with Eqs. (B.20) and (B.21) of Appendix B, is given by the transport equations of vorticity at the gyre and the jet scale, respectively:

$$\frac{\partial}{\partial t}\zeta^{\perp(L)} = \frac{2\Omega\sin\theta v_\theta^{(L)}}{r} + I^{\mathrm{conv}}\left(v_\theta^{(L)}, v_\phi^{(L)}\right) + (a_h + \nu_{Th}) I^h\left(v_\theta^{(L)}, v_\phi^{(L)}\right) + (a_v + \nu_{Tv}) I^v\left(v_\theta^{(L)}, v_\phi^{(L)}\right) + f_w^{(L)}, \tag{20}$$

$$\frac{\partial}{\partial t}\zeta^{\perp(l)} = \frac{2\Omega\sin\theta v_\theta^{(l)}}{r} + I^{\mathrm{conv}}\left(v_\theta^{(l)}, v_\phi^{(l)}\right) + a_h I^h\left(v_\theta^{(l)}, v_\phi^{(l)}\right) + a_v I^v\left(v_\theta^{(l)}, v_\phi^{(l)}\right) + f_w^{(l)}, \tag{21}$$

where $I^{\mathrm{conv}}\left(v_\theta^{(i)}, v_\phi^{(i)}\right)$, $I^h\left(v_\theta^{(i)}, v_\phi^{(i)}\right)$, $I^v\left(v_\theta^{(i)}, v_\phi^{(i)}\right)$ and $f_w^{(i)}$ are nonlinear convective terms, horizontal and vertical viscous and turbulence terms, and wind stress curl, respectively which are described in Appendix B. The jet-scale Eq. (21) is solved in the narrow strip representing the jet location and the gyre-scale Eq. (20) is solved in the entire double-gyre domain. The

jet-scale equations and the gyre-scale equations are completely decoupled from each other so, for simplicity, the full slip condition is imposed in each case:

$$v_\theta^{(L)}\left(\theta_j,\phi,t\right)=v_\phi^{(L)}\left(\theta,\phi_j,t\right)=0, v_\theta^{(l)}\left(\theta'_j,\phi,t\right)=v_\phi^{(l)}\left(\theta,\phi_j,t\right)=0,\ j=1,2. \tag{22}$$

The basis functions for the two-scale solution are obtained by using generalization in Eq. (19) to assumed single scale expansions in Eqs. (14) and (16)

$$\begin{aligned}
v_\theta^{(L)}&=\sum_{m=1}^{M}\sum_{n=1}^{N}Y_{mn}^{(L)}(t)\sin\left[m\omega_\theta(\theta-\theta_1)\right]\cos\left[(2n-1)\omega_\phi(\phi-\phi_1)\right],\\
v_\theta^{(l)}&=g(\theta'_1,\theta'_2)\sum_{m'=1}^{M'}\sum_{n'=1}^{N'}Y_{m'n'}^{(l)}(t)\sin\left[m'\omega'_\theta(\theta-\theta_1)\right]\cos\left[(2n'-1)\omega_\phi(\phi-\phi_1)\right],\\
v_\phi^{(L)}&=-\sum_{m=1}^{M}\sum_{n=1}^{N}\frac{Y_{mn}^{(L)}(t)}{(2n-1)\omega_\phi}\sin\left[(2n-1)\omega_\phi(\phi-\phi_1)\right]\\
&\times\left\{\cos\theta\sin\left[m\omega_\theta(\theta-\theta_1)\right]+m\omega_\theta\sin\theta\cos\left[m\omega_\theta(\theta-\theta_1)\right]\right\},\\
v_\phi^{(l)}&=-g(\theta'_1,\theta'_2)\sum_{m'=1}^{M'}\sum_{n'=1}^{N'}\frac{Y_{m'n'}^{(l)}(t)}{(2n-1)\omega_\phi}\sin\left[(2n'-1)\omega_\phi(\phi-\phi_1)\right]\\
&\times\left\{\cos\theta\sin\left[m'\omega'_\theta(\theta-\theta_1)\right]+m'\omega'_\theta\sin\theta\cos\left[m'\omega'_\theta(\theta-\theta_1)\right]\right\},
\end{aligned} \tag{23}$$

where $\omega'_\theta=\dfrac{2\pi}{\theta'_2-\theta'_1}$, $g(\theta'_1,\theta'_2)=H(\theta'_1)-H(\theta'_2)$ and $H(\theta'_1)$ and $H(\theta'_2)$ are the Heaviside step functions. Consequently, the weighting functions for the normal vorticity equations are given by:

$$\begin{aligned}
w_{ij}^{(L)}&=\frac{\sin\left[j\omega_\phi(\phi-\phi_1)\right]}{j\omega_\phi\sin\theta}\Big[j^2\omega_\phi{}^2\sin\left[i\omega_\theta(\theta-\theta_1)\right]-\cos^2\theta\sin\left[i\omega_\theta(\theta-\theta_1)\right]+\\
&\left(1+i^2\omega_\theta{}^2\right)\sin\left[i\omega_\theta(\theta-\theta_1)\right]\sin^2\theta-\frac{3i\omega_\theta\cos\left[i\omega_\theta(\theta-\theta_1)\right]\sin 2\theta}{2}\Big],\\
w_{i'j'}^{(l)}&=g(\theta'_1,\theta'_2)\frac{\sin\left[j'\omega_\phi(\phi-\phi_1)\right]}{j'\omega_\phi\sin\theta}\Big[j'^2\omega_\phi{}^2\sin\left[i'\omega'_\theta(\theta-\theta_1)\right]-\cos^2\theta\sin\left[i'\omega'_\theta(\theta-\theta_1)\right]+\\
&\left(1+i'^2\omega'^2_\theta\right)\sin\left[i'\omega'_\theta(\theta-\theta_1)\right]\sin^2\theta-\frac{3i'\omega'_\theta\cos\left[i'\omega'_\theta(\theta-\theta_1)\right]\sin 2\theta}{2}\Big],\\
&1\le i\le M,1\le j\le N,1\le i'\le M',1\le j'\le N'.
\end{aligned} \tag{24}$$

We multiply Eqs. 20 and 21 by the corresponding vorticity weighting functions (Eq. 24) for both jet and gyre-scale domains according to

$$w_{ij}^{(L)}.\left[\sum_{m=1}^{M}\sum_{n=1}^{N}\dot{Y}_{mn}^{(L)}(t)a_{mn}+\sum_{m=1}^{M}\sum_{n=1}^{N}Y_{mn}^{(L)}(t)b_{mn}+\sum_{m=1}^{M}\sum_{n=1}^{N}\left(\sum_{\mu=1}^{M}\sum_{\nu=1}^{N}Y_{\mu\nu}^{(L)}(t)c_{\mu\nu}\right)Y_{mn}^{(L)}(t)d_{mn}\right]=$$
$$\sum_{m=1}^{M}\sum_{n=1}^{N}\dot{Y}_{mn}^{(L)}(t)\left[w_{ij}^{(L)}.a_{mn}\right]+\sum_{m=1}^{M}\sum_{n=1}^{N}Y_{mn}^{(L)}(t)\left[w_{ij}^{(L)}.b_{mn}\right]+\sum_{m=1}^{M}\sum_{n=1}^{N}\sum_{\mu=1}^{M}\sum_{\nu=1}^{N}Y_{\mu\nu}^{(L)}(t)Y_{mn}^{(L)}(t)\left[w_{ij}^{(L)}.\left(c_{\mu\nu}d_{mn}\right)\right]=0,$$

$$w_{ij}^{(l)}.\left[\sum_{m'=1}^{M'}\sum_{n'=1}^{N'}\dot{Y}_{m'n'}^{(l)}(t)a_{m'n'}+\sum_{m'=1}^{M'}\sum_{n'=1}^{N'}Y_{m'n'}^{(l)}(t)b_{m'n'}+\sum_{m'=1}^{M'}\sum_{n'=1}^{N'}\left(\sum_{\mu=1}^{M'}\sum_{\nu=1}^{N'}Y_{\mu\nu}^{(l)}(t)c_{\mu\nu}\right)Y_{m'n'}^{(l)}(t)d_{m'n'}\right]=$$
$$\sum_{m'=1}^{M'}\sum_{n'=1}^{N'}\dot{Y}_{m'n'}^{(l)}(t)\left[w_{ij}^{(l)}.a_{m'n'}\right]+\sum_{m'=1}^{M'}\sum_{n'=1}^{N'}Y_{m'n'}^{(l)}(t)\left[w_{ij}^{(l)}.b_{m'n'}\right]+\sum_{m'=1}^{M'}\sum_{n'=1}^{N'}\sum_{\mu=1}^{M'}\sum_{\nu=1}^{N'}Y_{\mu\nu}^{(l)}(t)Y_{m'n'}^{(l)}(t)\left[w_{ij}^{(l)}.\left(c_{\mu\nu}d_{m'n'}\right)\right]=0. \quad (25)$$

and integrate the resulting equation over the grid of 128×128 elements in the (ϕ,θ)-domain to derive the final ODE system matrices as $\dot{\mathbf{Y}}+\mathbf{C}.\mathbf{Y}+\mathbf{N}(\mathbf{Y})=0$ where $\mathbf{Y}=\left[Y_{11}^{(L)}(t)\ \ .\ .\ .\ \ Y_{MN}^{(L)}(t)\ Y_{11}^{(l)}(t)\ \ .\ .\ .\ \ Y_{M'N'}^{(l)}(t)\right]^T$ and $1\le m\le M, 1\le n\le N$, $1\le m'\le M', 1\le n'\le N'$. Matrix $\mathbf{C}$ represents all linear terms of the weighted equation and $\mathbf{N}(\mathbf{Y})$ stands for a nonlinear vector resulting from all the convective and turbulence terms.

After solving the equations of each scale in time separately using a fourth-order Runge-Kutta scheme with integration time step equal to 2 days, the total velocity field in the entire double-gyre domain is found through superposition according to Eq. 19.

The computational program which achieves the spectral solution of the double-gyre problem is provided as supplementary materials to this article with the numerical implementation and programming details in appendix C.

5.3. Results

The solutions obtained are first investigated in terms of the spectral method convergence. It was first established that 9 terms of the spectral expansion (used in the rest of the simulations) are enough to obtain the solution within less than 0.2% variation as compared to the contribution of high-order terms.

Fig. 4 shows amplitudes of the 9 individual vorticity solution components normalised by the largest term for the gyre and the jet-scale solutions, $\zeta_{mn}^{\perp(L)}$ and $\zeta_{m'n'}^{\perp(l)}$, respectively, which are given by:

$$\zeta_{mn}^{\perp(L)} = \frac{Y_{mn}^{(L)}(t)}{r}\frac{\sin\left[n\omega_\phi(\phi-\phi_1)\right]}{n\omega_\phi\sin\theta}\Big[n^2\omega_\phi{}^2\sin\left[m\omega_\theta(\theta-\theta_1)\right]-\cos^2\theta\sin\left[m\omega_\theta(\theta-\theta_1)\right]$$

$$+\left(1+m^2\omega_\theta{}^2\right)\sin\left[m\omega_\theta(\theta-\theta_1)\right]\sin^2\theta-\frac{3m\omega_\theta\cos\left[m\omega_\theta(\theta-\theta_1)\right]\sin 2\theta}{2}\Big],$$

$$\zeta_{m'n'}^{\perp(l)} = g(\theta_1',\theta_2')\frac{Y_{m'n'}^{(l)}(t)}{r}\frac{\sin\left[n'\omega_\phi(\phi-\phi_1)\right]}{n'\omega_\phi\sin\theta}\Big[n'^2\omega_\phi{}^2\sin\left[m'\omega_\theta'(\theta-\theta_1)\right]-\cos^2\theta\sin\left[m'\omega_\theta'(\theta-\theta_1)\right]$$

$$+\left(1+m'^2\omega_\theta'{}^2\right)\sin\left[m'\omega_\theta'(\theta-\theta_1)\right]\sin^2\theta-\frac{3m'\omega_\theta'\cos\left[m'\omega_\theta'(\theta-\theta_1)\right]\sin 2\theta}{2}\Big],$$

$$1\le m\le M, 1\le n\le N, 1\le m'\le M', 1\le n'\le N', M=M'=N=N'=3.$$

(26)

The solutions presented in Fig. 4 are averaged over space and computed after the simulation was run over sufficiently long times (~5000 days) so that the temporal solution convergence was achieved similar to the single-scale Smagorinsky solution shown in Fig. 2. For better visibility, the two-dimensional indices of the solutions are represented by a single index running index in each case, $k=m+(n-1)M$ and $k'=m'+(n'-1)M'$ for the gyre-scale and the jet-scale solutions, respectively.

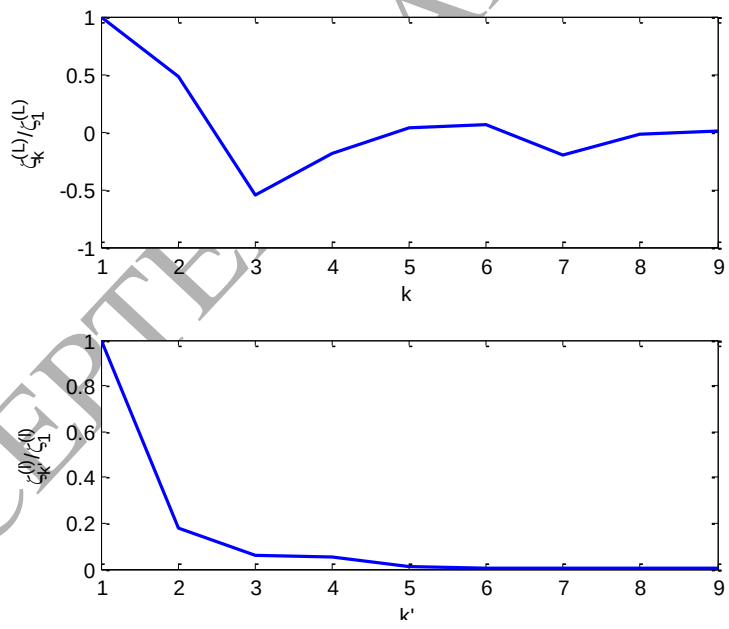

Fig. 4. Spectral convergence of the gyre- and jet- scale vorticity solution components.

In comparison with the single-scale spectral model based on the Smagorinsky eddy viscosity, the final two-scale model incorporates the new parameter that corresponds to the width of the jet flow region $\delta\theta=\theta_2'-\theta_1'$ with respect to the computational box size $(\theta_2-\theta_1)$.

By adjusting the Smagorinsky parameter and the jet region width parameter, the two-scale model captures both the integral angular momentum and the integral kinetic energy of the reference eddy-resolved double-gyre solution. The space of the operating parameters corresponding to the two-scale model and the single-scale Smagorinsky model from section 4 are shown in Fig. 5 as a function of the integral angular momentum and turbulent kinetic energy. The axes are made dimensionless with respect to the values of the reference eddy-resolving solution of the double-gyre problem. The reference integral values are obtained by averaging the corresponding unsteady eddy-resolving solution in space and time.

The integral parameters of the two-scale model exactly match those of the reference double-gyre solution for the set of calibration parameters $\delta\theta/(\theta_2-\theta_1)=0.354$ and $C_s=0.1$. These parameters are in a good agreement with a typical lateral size of the eddy-resolving jet solution in Fig. 1 and a recommended range of the Smagorinsky parameter value from the turbulence modelling literature, respectively. In contrast with this, the single-scale Smagorinsky model cannot be informed by the eddy-resolving solution to fully agree with the reference "true" parameters: the integral kinetic energy is too low or the angular momentum is much higher as compared to the "truth".

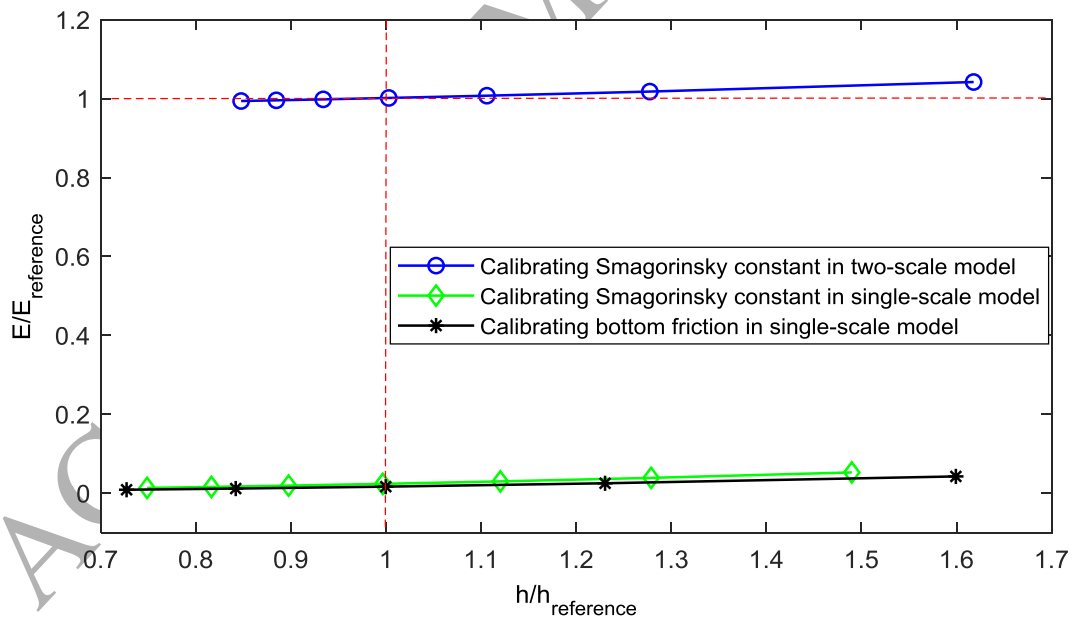

Fig. 5. The integral kinetic energy and angular momentum parameter space of the double-gyre problem as compared to the reference eddy-resolving solution: the single-scale Smagorinsky solutions for various Smagorinsky and bottom friction viscosity parameters

(green and black lines) vs the two-scale solutions for various Smagorinsky viscosity parameters (blue lines).

As a further validation step of the two-scale model, its mean-flow velocity profile is compared with the reference eddy-resolving solution. Notably, being an approximate model, the two-scale solution only captures the average parallel flow aspect of the full meandering jet solution of the eddy-resolving model. This means that the two-scale solution is essentially averaged in the zonal direction as compared to the latter. Hence, Fig. 6 compares the solution of the two-scale model for the zonal velocity profile, v_ϕ with the layer- and time-averaged solution of the eddy-resolving simulation that was also averaged over the half of the domain in the zonal direction $\left(\phi_1,(\phi_1+\phi_2)/2\right)$ to fully include the jet in accordance with Fig. 1.

This comparison shows that the two-scale model captures the jet profile quite well. Besides the jet shape, the semi-analytical solution even predicts the two recirculation zones, which appear above and below the jet in the reference eddy-resolving solution. Further features of the eddy-resolving solution outside the primary jet region, such as the secondary jet excursions near the top and the bottom boundaries, are averaged out in the semi-analytical two-scale model. All of this shows that the two-scale model correctly predicts the primary features of the jet flow quite well and generally reproduces the latitude-wise averaged state of the reference eddy resolving solution outside of the jet region.

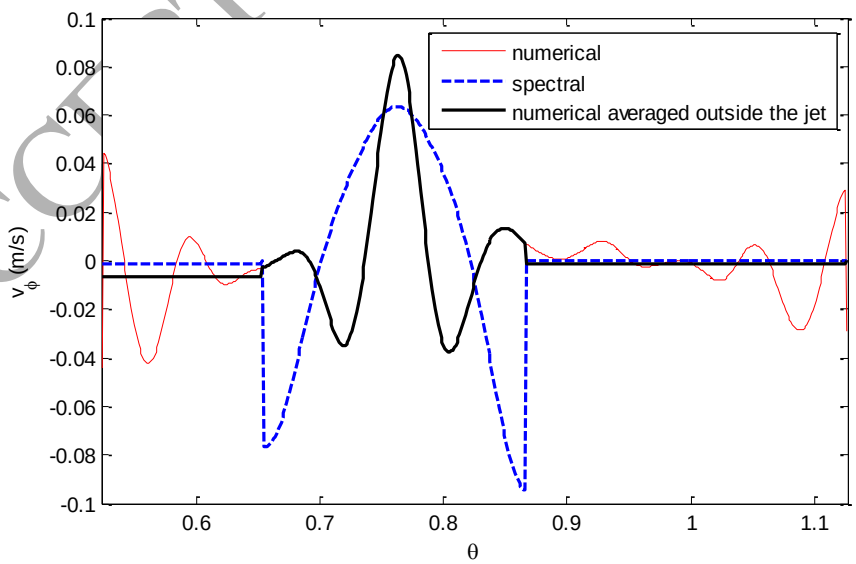

Fig. 6. Comparison of the zonal velocity profile: the two-scale model versus the reference eddy-resolving solution. The velocity profiles of both models are averaged zonally along the jet flow direction between ϕ_1 and $(\phi_1 + \phi_2)/2$.

6. Conclusion

For a double-gyre problem in a meso-scale regime which is characterised by an eastward jet flow separating from the west boundary under the stationary wind forcing effect, several semi-analytical models have been considered: a single-scale model with linear viscosity, a single-scale model incorporating nonlinear eddy viscosity approximation and a two-scale model with nonlinear eddy viscosity. All models correspond to solving the depth-averaged Navier-Stokes equations using a spectral Galerkin approach with and without the eddy-viscosity parameterisation based on the Smagorinsky model. In comparison with the linear-eddy viscosity model, the Smagorinsky parameterisation allows converged solutions to be obtained for a turbulent flow solution regime. Still, regardless of the choice of the calibration parameters, the turbulent diffusion parameterisation by itself cannot either represent the most important dynamic feature of the double-gyre, that is the jet, or satisfy to the correct integral angular momentum and the integral kinetic energy properties of the system at the same time. Therefore, an improved two-scale semi-analytical model is suggested that is inspired by the multi-scale idea of scale separation between the jet that consists of coherent vortices and the surrounding much less correlated flow. Despite the simplicity, the two-scale model captures both the integral angular momentum and the integral kinetic energy of the double-gyre system respectively within 0.25% and 0.5% error bar as compared to the reference eddy-resolving solution of the double-gyre problem. Moreover, the semi-analytical model correctly represents the jet mean-flow velocity profile and the spatially averaged state of the surrounding flow as compared to the reference solution.

The consistency of the developed low-fidelity model in predicting mean velocity and vorticity distributions as well as overall kinetic energy and angular momentum highlights the fact that the two-scale governing equations and the spectral basis functions reflect the key physical characteristics of the double-gyre problem correctly. The current model can be further extended to better capture local features of the evolving jet by introducing additional parameters such as the tilt of the jet zone and its zonal length dependency on viscosity parameters [13]. This extension together with further refined basis functions is the direction which we would like to pursue in our future work.

The two-scale model together with its semi-analytical solutions developed can be used as a toy Navier-Stokes model to rapidly explore the parameter space in application to global geophysical flow simulations such as in [30]. The computational program achieving quick turn-around-time spectral solutions of the double-gyre problem (the block-scheme of which is outlined in Appendix C) is provided as supplementary materials to this article.

Acknowledgement

Funding from Partnership for Observation of Global Oceans and Scientific Committee for Oceanic Research (POGO-SCOR) is acknowledged by S.E.N. with gratitude. The work of S.K. was supported by Natural Environment Research Council grant (NE/H020837/1).

The authors are thankful to Drs Shevchenko and Berloff from Imperial College London for making their quasi-geostrophic double-gyre code readily available. The use of computing resource on Apocrita computer cluster in Queen Mary University of London is appreciatively acknowledged.

Appendix A: Stratified quasi-geostrophic equations and their reduction to the idealized layer-averaged equation for the double-gyre problem

Here, we present how stratified quasi-geostrophic potential vorticity equations can be derived from three dimensional Navier-Stokes equations. To this end, we start with the general Navier-Stokes momentum and continuity equations described in Eq. (1)

$$\frac{\partial \mathbf{v}}{\partial t}+(\mathbf{v}.\nabla)\mathbf{v}+\boldsymbol{\omega}(\boldsymbol{\omega}\times\mathbf{r})+2\boldsymbol{\omega}\times\mathbf{v}=\mathbf{g}-\frac{\nabla P}{\rho}+\frac{\nabla.\boldsymbol{\tau}}{\rho}+\frac{\mathbf{T}}{h_w},\qquad \text{(A.1)}$$
$$\nabla.\mathbf{v}=0.$$

Using material derivative notation and combining centrifugal terms and gravitational acceleration, we can alternatively write the Navier-Stokes momentum equation in the compact form as below

$$\frac{D\mathbf{v}}{Dt}+2\boldsymbol{\omega}\times\mathbf{v}=\mathbf{g}'-\frac{\nabla P}{\rho}+\frac{\nabla.\boldsymbol{\tau}}{\rho}+\frac{\mathbf{T}}{h_w},\qquad \text{(A.2)}$$

where $\mathbf{g}'=\mathbf{g}-\boldsymbol{\omega}(\boldsymbol{\omega}\times\mathbf{r})$.

In geostrophic currents, forcing, dissipation and temporal terms are ignored; hence, the geostrophic balance can be written as the balance of Coriolis terms and pressure gradients

$$2\boldsymbol{\omega}\times\mathbf{v}_g=\mathbf{g}'-\frac{\nabla P}{\rho}, \tag{A.3}$$

where subscript *g* denotes geostrophic and $\mathbf{v}_g=\left[u_g,v_g,0\right]^{\mathrm{T}}$. In component form, we have

$$f_0 v_g=\frac{1}{\rho}\frac{\partial p}{\partial x},\ f_0 u_g=-\frac{1}{\rho}\frac{\partial p}{\partial y},\ g'=\frac{1}{\rho}\frac{\partial p}{\partial z}, \tag{A.4}$$

where $f_0=2\Omega\sin\theta_0$ is the Coriolis parameter. Furthermore, since geostrophic flow is two dimensional, velocity components can be expressed in terms of stream function ψ

$$u_g=-\frac{\partial\psi}{\partial y},v_g=\frac{\partial\psi}{\partial x},w_g=0,g'=f_0\frac{\partial\psi}{\partial z}, \tag{A.5}$$

and geostrophic vorticity is defined as the *z* component of the geostrophic velocity curl

$$\zeta_g=\frac{\partial v_g}{\partial x}-\frac{\partial u_g}{\partial y}=\nabla^2\psi. \tag{A.6}$$

In quasi-geostrophic currents, advection terms cannot be neglected and are considered as the next terms in order of magnitude after Coriolis terms and pressure gradients. To drive quasi-geostrophic equations, we perturb the geostrophic velocity field with an ageostrophic component

$$\mathbf{v}=\mathbf{v}_g+\mathbf{v}_a, \tag{A.7}$$

and also perturb the Coriolis parameter as below

$$f=2\Omega\sin\theta=2\Omega\left(\sin\theta_0+\cos\theta_0\Delta\theta+...\right)\simeq f_0+\beta y\ , \tag{A.8}$$

where $\left|\mathbf{v}_a\right|<<\left|\mathbf{v}_g\right|$ and $\beta y<<f_0$.

Now, let's rewrite the first two components of Eq. (A.2) in terms of perturbed variables

$$\begin{aligned}\frac{Du_g}{Dt}-f_0v_a-\beta yv_g&=a_h\left(\frac{\partial^2u_g}{\partial x^2}+\frac{\partial^2u_g}{\partial y^2}\right)+a_v\frac{\partial^2u_g}{\partial z^2}+\frac{T_x}{h_w},\\ \frac{Dv_g}{Dt}+f_0u_a+\beta yu_g&=a_h\left(\frac{\partial^2v_g}{\partial x^2}+\frac{\partial^2v_g}{\partial y^2}\right)+a_v\frac{\partial^2v_g}{\partial z^2}+\frac{T_y}{h_w}.\end{aligned} \tag{A.9}$$

In deriving the above equations, the geostrophic kernel disappears according to A.4, linear terms are retained and all quadratic combinations of perturbed variables are neglected [36]. Taking curl of the above equations leads to

$$\frac{D\zeta_g}{Dt}+f_0\left(\frac{\partial u_a}{\partial x}+\frac{\partial v_a}{\partial y}\right)+\beta v_g+\beta\left(\frac{\partial u_g}{\partial x}+\frac{\partial v_g}{\partial y}\right)=a_h\left(\frac{\partial^2\zeta_g}{\partial x^2}+\frac{\partial^2\zeta_g}{\partial y^2}\right)+a_v\frac{\partial^2\zeta_g}{\partial z^2}+F_w. \quad \text{(A.10)}$$

where $F_w=\frac{1}{h_w}\left(\frac{\partial T_y}{\partial x}-\frac{\partial T_x}{\partial y}\right)$ and we can approximate $\frac{\partial^2\zeta_g}{\partial z^2}=\frac{\zeta_g}{h_b^{\,2}}$ (h_b is the bottom boundary layer depth). We also have $\frac{D(\beta y)}{Dt}=\beta v_g$ and $\frac{\partial u_g}{\partial x}+\frac{\partial v_g}{\partial y}=0$ and since the ageostrophic velocity satisfies the continuity equation

$$\frac{\partial u_a}{\partial x}+\frac{\partial v_a}{\partial y}+\frac{\partial w_a}{\partial z}=0, \quad \text{(A.11)}$$

we can achieve

$$f_0\left(\frac{\partial u_a}{\partial x}+\frac{\partial v_a}{\partial y}\right)=-f_0\frac{\partial w_a}{\partial z}. \quad \text{(A.12)}$$

Moreover, from quasi-geostrophic thermodynamics equations [36]

$$\frac{D}{Dt}\left(f_0\frac{\partial\psi}{\partial z}\right)+N_0^{\,2}w_a=0, \quad \text{(A.13)}$$

we can deduce

$$-f_0\frac{\partial w_a}{\partial z}=\frac{D}{Dt}\frac{\partial}{\partial z}\left(\frac{f_0^{\,2}}{N_0^{\,2}}\frac{\partial\psi}{\partial z}\right). \quad \text{(A.14)}$$

where is N_0 the buoyancy frequency. Hence, the governing equation for quasi-geostrophic currents can be written as

$$\frac{Dq}{Dt}=a_h\nabla^4\psi+\frac{a_v}{h_b^{\,2}}\nabla^2\psi+F_w, \quad \text{(A.15)}$$

where q is the quasi-geostrophic potential vorticity defined as

$$q = \nabla^2 \psi + \beta y + \frac{\partial}{\partial z}\left(\frac{{f_0}^2}{{N_0}^2} \frac{\partial \psi}{\partial z} \right). \tag{A.16}$$

In ocean modelling literature, the bottom friction term in Eq. (A.15) commonly appears with a minus due to a left-hand choice of the coordinate system [13].

In stratified quasi-geostrophic potential vorticity equations such as the ones used in this paper as the reference model (Eq. (2)), a centred finite difference discretization is utilized in the vertical dimension and the resulting system of equations to relate vorticity and stream function are

$$\mathbf{Z} = \nabla^2 \boldsymbol{\psi} + S\boldsymbol{\psi}, \tag{A.17}$$

where $\mathbf{Z} = \left[z_1 \quad . \quad . \quad . \quad z_N \right]^{\mathrm{T}}$, $\boldsymbol{\psi} = \left[\psi_1 \quad . \quad . \quad . \quad \psi_N \right]^{\mathrm{T}}$, $z_i = q_i - \beta y$ and N is the number of layers. S is the stratification matrix with elements described as below

$$\sum_{j=1}^{N} S_{ij}\psi_j = \begin{array}{ll} s_1^{+}\left(\psi_2 - \psi_1\right), & i = 1, \\ s_i^{-}\left(\psi_{i-1} - \psi_i\right) + s_i^{+}\left(\psi_{i+1} - \psi_i\right), & 1 < i < N, \\ s_N^{-}\left(\psi_{i-1} - \psi_i\right), & i = N, \end{array} \tag{A.18}$$

where

$$s_i^{+} = \frac{{f_0}^2}{{N_{i+1/2}}^2} \frac{2}{h_i\left(h_{i+1} + h_i\right)}, s_i^{-} = \frac{{f_0}^2}{{N_{i-1/2}}^2} \frac{2}{h_i\left(h_{i-1} + h_i\right)}. \tag{A.19}$$

$N_{i\text{-}1/2}$ is the buoyancy frequency at the interface between the i-1 and ith levels and so is $N_{i+1/2}$ defined between the i+1 and ith levels

$${N_{i+1/2}}^2 = \frac{2g'_{i+1/2}}{\left(h_{i+1} + h_i\right)}, {N_{i-1/2}}^2 = \frac{2g'_{i-1/2}}{\left(h_{i-1} + h_i\right)}, \tag{A.20}$$

and

$$g'_{i+1/2} = -g\frac{\rho_i - \rho_{i+1}}{\rho_0}, g'_{i-1/2} = -g\frac{\rho_{i-1} - \rho_i}{\rho_0}. \tag{A.21}$$

Equations (A.17) are decoupled as below

$$D\mathbf{Z} = \nabla^2 D\boldsymbol{\psi} + DS\boldsymbol{\psi}, \tag{A.22}$$

using the modal matrix D which diagonalizes the stratification matrix

$$\begin{aligned} &DSD^{-1} = \Lambda, \\ &\Lambda = \mathrm{diag}\left[\lambda_1 \quad . \quad . \quad . \quad \lambda_N\right]. \end{aligned} \tag{A.23}$$

In terms of transformed variables $\tilde{\mathbf{Z}} = D\mathbf{Z}$ and $\tilde{\boldsymbol{\psi}} = D\boldsymbol{\psi}$, the governing equations will be

$$\tilde{\mathbf{Z}} = \nabla^2\tilde{\boldsymbol{\psi}} + \Lambda\tilde{\boldsymbol{\psi}}, \tag{A.24}$$

and in component form

$$\tilde{z}_i = \left(\nabla^2 + \lambda_i\right)\tilde{\psi}_i, \tag{A.25}$$

where λ_i is the ith eigenvalue of S and is defined in terms of Rossby radii of deformation $R_{D,i}$

$$\lambda_i = -\frac{1}{{R_{D,i}}^2}. \tag{A.26}$$

It should be noted that for a stratified quasi-geostrophic model wind stress is applied on the top layer and bottom friction is applied on the bottom layer ($h_w = h_1, h_b = h_N$).

To develop a layer-averaged model, we first simplify Eq. (A.10) as

$$\frac{D\zeta_g}{Dt} - f_0\frac{\partial w_a}{\partial z} + \beta v_g = a_h\left(\frac{\partial^2\zeta_g}{\partial x^2} + \frac{\partial^2\zeta_g}{\partial y^2}\right) + \frac{a_v}{{h_N}^2}\zeta_g + F_w, \tag{A.27}$$

and then the depth-averaged equation is achieved by finding the integration mean value

$$\frac{D\overline{\zeta}_g}{Dt} - \frac{f_0 w_a}{H}\Big|_0^H + \beta\overline{v}_g = a_h\left(\frac{\partial^2\overline{\zeta}_g}{\partial x^2} + \frac{\partial^2\overline{\zeta}_g}{\partial y^2}\right) + \frac{a_v}{{h_N}^2}\frac{h_N}{H}\overline{\zeta}_g + \frac{h_1}{H}F_w. \tag{A.28}$$

Based on the problem's boundary conditions, there is no cross flow through the rigid walls surrounding and beneath the solution domain

$$\begin{aligned} &u_a\left(0,y,z\right) = u_a\left(L,y,z\right) = 0, \\ &v_a\left(x,0,z\right) = v_a\left(x,L,z\right) = 0, \\ &w_a\left(x,y,0\right) = 0, \end{aligned} \tag{A.29}$$

and combining continuity equation and divergence theorem for the ageostrophic velocity

$$\iint_A \mathbf{v}_a.\mathbf{n} = \iiint_V \nabla.\mathbf{v}_a = 0, \tag{A.30}$$

we conclude $w_a(x,y,H)=0$ and hence $\frac{f_0 w_a}{H}|_0^H=0$, which yields

$$\frac{D\overline{\zeta}_g}{Dt}+\beta\overline{v}_g=a_h\left(\frac{\partial^2\overline{\zeta}_g}{\partial x^2}+\frac{\partial^2\overline{\zeta}_g}{\partial y^2}\right)+\frac{a_v}{{h_N}^2}\frac{h_N}{H}\overline{\zeta}_g+\frac{h_1}{H}F_w. \tag{A.31}$$

The above equation is Cartesian expression of the layer-averaged equation used as the simplified double-gyre model and Eqs. (A.27) to (A.31) illustrate how the two models used in this paper are translated to one another in terms of the involved terms and their corresponding coefficients. It should also be noticed that in spherical coordinates, θ is handled as a variable and β-plane approximation (Eq. (A.8)) is irrelevant.

Appendix B: Two-scale model approximation of the double-gyre problem

Let's consider the Navier-Stokes momentum equations for incompressible viscous rotating flow in a latitude-longitude quadrangle $\theta_1<\theta<\theta_2,\phi_1<\phi<\phi_2$

$$\begin{aligned}
&\frac{\partial v_\theta}{\partial t}-2\Omega v_\phi\cos\theta+\frac{v_\theta}{r}\frac{\partial v_\theta}{\partial\theta}+\frac{v_\phi}{r\sin\theta}\frac{\partial v_\theta}{\partial\phi}-\frac{{v_\phi}^2\cot\theta}{r}=\\
&-\frac{1}{\rho r}\frac{\partial P}{\partial\theta}+a_v\left(\frac{\partial^2 v_\theta}{\partial r^2}+\frac{2}{r}\frac{\partial v_\theta}{\partial r}\right)+a_h\left[\frac{1}{r^2}\frac{\partial}{\partial\theta}\left(\frac{1}{\sin\theta}\frac{\partial}{\partial\theta}\left(v_\theta\sin\theta\right)\right)+\frac{1}{r^2\sin^2\theta}\frac{\partial^2 v_\theta}{\partial\phi^2}-\frac{2\cot\theta}{r^2\sin\theta}\frac{\partial v_\phi}{\partial\phi}\right],\\
&\frac{\partial v_\phi}{\partial t}+2\Omega v_\theta\cos\theta+\frac{v_\theta}{r}\frac{\partial v_\phi}{\partial\theta}+\frac{v_\phi}{r\sin\theta}\frac{\partial v_\phi}{\partial\phi}+\frac{v_\phi v_\theta\cot\theta}{r}=\\
&-\frac{1}{\rho r\sin\theta}\frac{\partial P}{\partial\phi}+a_v\left(\frac{\partial^2 v_\phi}{\partial r^2}+\frac{2}{r}\frac{\partial v_\phi}{\partial r}\right)+a_h\left[\frac{1}{r^2}\frac{\partial}{\partial\theta}\left(\frac{1}{\sin\theta}\frac{\partial}{\partial\theta}\left(v_\phi\sin\theta\right)\right)+\frac{1}{r^2\sin^2\theta}\frac{\partial^2 v_\phi}{\partial\phi^2}+\frac{2\cot\theta}{r^2\sin\theta}\frac{\partial v_\theta}{\partial\phi}\right].
\end{aligned} \tag{B.1}$$

A particular solution to these equations is considered that incorporates two distinctly different scales in space and time. These are the jet scales l,τ and the gyre scales L,T which respectively correspond to a narrow strip of the domain comprising the jet in the longitudinal direction and the surrounding flow of the double-gyre configuration. The velocity field is represented as a sum of the velocity components in the two scales so that

$$\begin{aligned}
&v_\theta={v_\theta}^{(L)}+{v_\theta}^{(l)},v_\phi={v_\phi}^{(L)}+{v_\phi}^{(l)},\\
&l/L=\tau/T=\varepsilon<<1,
\end{aligned}. \tag{B.2}$$

$$\theta_c-\frac{l_0}{L_0}\frac{\Delta\theta}{2}<\theta^{(l)}<\theta_c+\frac{l_0}{L_0}\frac{\Delta\theta}{2},\ \phi_1<\phi^{(l)}<\phi_2, \tag{B.3}$$

where θ_c is the jet centreline coordinate in accordance with the jet separation point at the west boundary, $\Delta\theta = \theta_2 - \theta_1$ and L_0 and l_0 are meridional dimensions of the gyre scale and jet scale solution zones respectively. We also assume that the variation and amplitude in the jet-scale solution are both much larger as compared to the gyre-scale solution

$$\frac{\left|v_\theta^{(L)}\right|}{\left|v_\theta^{(l)}\right|} = \frac{\left|v_\phi^{(L)}\right|}{\left|v_\phi^{(l)}\right|} = \delta << 1. \tag{B.4}$$

Substituting Eq. (B.2) into the original Eqs. (B.1) yields

$$\begin{aligned}
&\frac{\partial\left(v_\theta^{(L)}+v_\theta^{(l)}\right)}{\partial t} - 2\Omega\left(v_\phi^{(L)}+v_\phi^{(l)}\right)\cos\theta + \frac{\left(v_\theta^{(L)}+v_\theta^{(l)}\right)}{r}\frac{\partial\left(v_\theta^{(L)}+v_\theta^{(l)}\right)}{\partial\theta} + \frac{\left(v_\phi^{(L)}+v_\phi^{(l)}\right)}{r\sin\theta}\frac{\partial\left(v_\theta^{(L)}+v_\theta^{(l)}\right)}{\partial\phi} \\
&-\frac{\left(v_\phi^{(L)}+v_\phi^{(l)}\right)^2\cot\theta}{r} = -\frac{1}{\rho r}\frac{\partial\left(p^{(L)}+p^{(l)}\right)}{\partial\theta} + a_v\left(\frac{\partial^2\left(v_\theta^{(L)}+v_\theta^{(l)}\right)}{\partial r^2} + \frac{2}{r}\frac{\partial\left(v_\theta^{(L)}+v_\theta^{(l)}\right)}{\partial r}\right) \\
&+a_h\left[\frac{1}{r^2}\frac{\partial}{\partial\theta}\left(\frac{1}{\sin\theta}\frac{\partial}{\partial\theta}\left(\left(v_\theta^{(L)}+v_\theta^{(l)}\right)\sin\theta\right)\right) + \frac{1}{r^2\sin^2\theta}\frac{\partial^2\left(v_\theta^{(L)}+v_\theta^{(l)}\right)}{\partial\phi^2} - \frac{2\cot\theta}{r^2\sin\theta}\frac{\partial\left(v_\phi^{(L)}+v_\phi^{(l)}\right)}{\partial\phi}\right], \\
&\frac{\partial\left(v_\phi^{(L)}+v_\phi^{(l)}\right)}{\partial t} + 2\Omega\left(v_\theta^{(L)}+v_\theta^{(l)}\right)\cos\theta + \frac{\left(v_\theta^{(L)}+v_\theta^{(l)}\right)}{r}\frac{\partial\left(v_\phi^{(L)}+v_\phi^{(l)}\right)}{\partial\theta} + \frac{\left(v_\phi^{(L)}+v_\phi^{(l)}\right)}{r\sin\theta}\frac{\partial\left(v_\phi^{(L)}+v_\phi^{(l)}\right)}{\partial\phi} \\
&+\frac{\left(v_\phi^{(L)}+v_\phi^{(l)}\right)\left(v_\theta^{(L)}+v_\theta^{(l)}\right)\cot\theta}{r} = -\frac{1}{\rho r\sin\theta}\frac{\partial\left(p^{(L)}+p^{(l)}\right)}{\partial\phi} + a_v\left(\frac{\partial^2\left(v_\phi^{(L)}+v_\phi^{(l)}\right)}{\partial r^2} + \frac{2}{r}\frac{\partial\left(v_\phi^{(L)}+v_\phi^{(l)}\right)}{\partial r}\right) \\
&+a_h\left[\frac{1}{r^2}\frac{\partial}{\partial\theta}\left(\frac{1}{\sin\theta}\frac{\partial}{\partial\theta}\left(\left(v_\phi^{(L)}+v_\phi^{(l)}\right)\sin\theta\right)\right) + \frac{1}{r^2\sin^2\theta}\frac{\partial^2\left(v_\phi^{(L)}+v_\phi^{(l)}\right)}{\partial\phi^2} + \frac{2\cot\theta}{r^2\sin\theta}\frac{\partial\left(v_\theta^{(L)}+v_\theta^{(l)}\right)}{\partial\phi}\right].
\end{aligned} \tag{B.5}$$

Next, (B.5) is made dimensionless through using (B.2) and (B.4)

$$\begin{aligned}
&v_\theta^{(L)}, v_\phi^{(L)} \to U v_\theta^{*(L)}, U v_\phi^{*(L)}; v_\theta^{(l)}, v_\phi^{(l)} \to U/\delta\cdot v_\theta^{*(l)}, U/\delta\cdot v_\phi^{*(l)}; U = \max(v_\theta^{(L)}, v_\phi^{(L)}), \\
&r\partial\theta^{(L)}, r\partial\phi^{(L)}, \partial t^{(L)} \to L\cdot r^*\partial\theta^{*(L)}, L\cdot r^*\partial\phi^{*(L)}, T\cdot\partial t^{*(L)}, \\
&r\partial\theta^{(l)}, r\partial\phi^{(l)}, \partial t^{(l)} \to \varepsilon\cdot L\cdot r^*\partial\theta^{*(l)}, \varepsilon\cdot L\cdot r^*\partial\phi^{*(l)}, \varepsilon\cdot T\cdot\partial t^{*(l)},
\end{aligned} \tag{B.6}$$

which, after some re-arrangement, leads to the following equations for the latitudinal and longitudinal velocity components:

$$\left\{\frac{U}{T}\frac{\partial v_\theta^{*(L)}}{\partial t^{*(L)}} - 2U\Omega v_\phi^{*(L)}\cos\theta + \frac{U}{L}\frac{v_\theta}{r^*}\frac{\partial v_\theta^{*(L)}}{\partial\theta^{*(L)}} + \frac{U}{L}\frac{v_\phi}{r^*\sin\theta}\frac{\partial v_\theta^{*(L)}}{\partial\phi^{*(L)}} - \frac{U}{L}\frac{v_\phi v_\phi^{*(L)}\cot\theta}{r^*} + \frac{P}{\rho r^* L}\frac{\partial p^{*(L)}}{\partial\theta^{*(L)}}\right.$$
$$\left. - \frac{a_v U}{R^2}\left(\frac{\partial^2 v_\theta^{*(L)}}{\partial r^{*2}} + \frac{2}{r^*}\frac{\partial v_\theta^{*(L)}}{\partial r^*}\right) - \frac{a_h U}{L^2}\left[\frac{1}{r^{*2}}\frac{\partial}{\partial\theta^{*(L)}}\left(\frac{1}{\sin\theta}\frac{\partial}{\partial\theta^{*(L)}}\left(v_\theta^{*(L)}\sin\theta\right)\right) + \frac{1}{r^{*2}\sin^2\theta}\frac{\partial^2 v_\theta^{*(L)}}{\partial\phi^{*(L)2}} - \frac{2\cot\theta}{r^{*2}\sin\theta}\frac{\partial v_\phi^{*(L)}}{\partial\phi^{*(L)}}\right]\right\}$$
$$+\frac{1}{\varepsilon\delta}\left\{\frac{U}{T}\frac{\partial v_\theta^{*(l)}}{\partial t^{*(l)}} - 2\varepsilon\Omega v_\phi^{*(l)}\cos\theta + \frac{U}{L}\frac{v_\theta}{r^*}\frac{\partial v_\theta^{*(l)}}{\partial\theta^{*(l)}} + \frac{U}{L}\frac{v_\phi}{r^*\sin\theta}\frac{\partial v_\theta^{*(l)}}{\partial\phi^{*(l)}} - \frac{U}{L}\frac{v_\phi v_\phi^{*(l)}\cot\theta}{r^*} + \frac{P}{\rho r^* L}\frac{\partial p^{*(l)}}{\partial\theta^{*(l)}}\right.$$
$$\left. - \varepsilon\frac{a_v U}{R^2}\left(\frac{\partial^2 v_\theta^{*(l)}}{\partial r^{*2}} + \frac{2}{r^*}\frac{\partial v_\theta^{*(l)}}{\partial r^*}\right) - \frac{1}{\varepsilon}\frac{a_h U}{L^2}\left[\frac{1}{r^{*2}}\frac{\partial}{\partial\theta^{*(l)}}\left(\frac{1}{\sin\theta}\frac{\partial}{\partial\theta^{*(l)}}\left(v_\theta^{*(l)}\sin\theta\right)\right) + \frac{1}{r^{*2}\sin^2\theta}\frac{\partial^2 v_\theta^{*(l)}}{\partial\phi^{*(l)2}} - \frac{2\cot\theta}{r^{*2}\sin\theta}\frac{\partial v_\phi^{*(l)}}{\partial\phi^{*(l)}}\right]\right\},$$

$$\left\{\frac{U}{T}\frac{\partial v_\phi^{*(L)}}{\partial t^{*(L)}} + 2U\Omega v_\theta^{*(L)}\cos\theta + \frac{U}{L}\frac{v_\theta}{r^*}\frac{\partial v_\phi^{*(L)}}{\partial\theta^{*(L)}} + \frac{U}{L}\frac{v_\phi}{r^*\sin\theta}\frac{\partial v_\phi^{*(L)}}{\partial\phi^{*(L)}} + \frac{U}{L}\frac{v_\phi v_\theta^{*(L)}\cot\theta}{r^*} + \frac{P}{\rho r^* L\sin\theta}\frac{\partial p^{*(L)}}{\partial\phi^{*(L)}}\right.$$
$$\left. - \frac{a_v U}{R^2}\left(\frac{\partial^2 v_\phi^{*(L)}}{\partial r^{*2}} + \frac{2}{r^*}\frac{\partial v_\phi^{*(L)}}{\partial r^*}\right) - \frac{a_h U}{L^2}\left[\frac{1}{r^{*2}}\frac{\partial}{\partial\theta^{*(L)}}\left(\frac{1}{\sin\theta}\frac{\partial}{\partial\theta^{*(L)}}\left(v_\phi^{*(L)}\sin\theta\right)\right) + \frac{1}{r^{*2}\sin^2\theta}\frac{\partial^2 v_\phi^{*(L)}}{\partial\phi^{*(L)2}} + \frac{2\cot\theta}{r^{*2}\sin\theta}\frac{\partial v_\theta^{*(L)}}{\partial\phi^{*(L)}}\right]\right\}$$
$$+\frac{1}{\delta\varepsilon}\left\{\frac{U}{T}\frac{\partial v_\phi^{*(l)}}{\partial t^{*(l)}} + 2\varepsilon U\Omega v_\theta^{*(l)}\cos\theta + \frac{U}{L}\frac{v_\theta}{r^*}\frac{\partial v_\phi^{*(l)}}{\partial\theta^{*(l)}} + \frac{U}{L}\frac{v_\phi}{r^*\sin\theta}\frac{\partial v_\phi^{*(l)}}{\partial\phi^{*(l)}} + \frac{U}{L}\frac{v_\phi v_\theta^{*(l)}\cot\theta}{r^*} + \frac{P}{\rho r^* L\sin\theta}\frac{\partial p^{*(l)}}{\partial\phi^{*(l)}}\right.$$
$$\left. - \varepsilon\frac{a_v U}{R^2}\left(\frac{\partial^2 v_\phi^{*(l)}}{\partial r^{*2}} + \frac{2}{r^*}\frac{\partial v_\phi^{*(l)}}{\partial r^*}\right) - \frac{1}{\varepsilon}\frac{a_h U}{L^2}\left[\frac{1}{r^{*2}}\frac{\partial}{\partial\theta^{*(l)}}\left(\frac{1}{\sin\theta}\frac{\partial}{\partial\theta^{*(l)}}\left(v_\phi^{*(l)}\sin\theta\right)\right) + \frac{1}{r^{*2}\sin^2\theta}\frac{\partial^2 v_\phi^{*(l)}}{\partial\phi^{*(l)2}} + \frac{2\cot\theta}{r^{*2}\sin\theta}\frac{\partial v_\theta^{*(l)}}{\partial\phi^{*(l)}}\right]\right\} = 0. \tag{B.7}$$

Assuming scale separation, Eqs. (B.7) are decomposed into two separate sets of equations in terms of the gyre-scale and the jet-scale components:

$$\frac{\partial v_\theta^{(L)}}{\partial t} - 2\Omega v_\phi^{(L)}\cos\theta + \frac{v_\theta}{r}\frac{\partial v_\theta^{(L)}}{\partial\theta} + \frac{v_\phi}{r\sin\theta}\frac{\partial v_\theta^{(L)}}{\partial\phi} - \frac{v_\phi v_\phi^{(L)}\cot\theta}{r} + \frac{1}{\rho r}\frac{\partial P^{(L)}}{\partial\theta}$$
$$-a_v\left(\frac{\partial^2 v_\theta^{(L)}}{\partial r^2} + \frac{2}{r}\frac{\partial v_\theta^{(L)}}{\partial r}\right) - a_h\left[\frac{1}{r^2}\frac{\partial}{\partial\theta}\left(\frac{1}{\sin\theta}\frac{\partial}{\partial\theta}\left(v_\theta^{(L)}\sin\theta\right)\right) + \frac{1}{r^2\sin^2\theta}\frac{\partial^2 v_\theta^{(L)}}{\partial\phi^2} - \frac{2\cot\theta}{r^2\sin\theta}\frac{\partial v_\phi^{(L)}}{\partial\phi}\right] = 0,$$

$$\frac{\partial v_\phi^{(L)}}{\partial t} + 2\Omega v_\theta^{(L)}\cos\theta + \frac{v_\theta}{r}\frac{\partial v_\phi^{(L)}}{\partial\theta} + \frac{v_\phi}{r\sin\theta}\frac{\partial v_\phi^{(L)}}{\partial\phi} + \frac{v_\phi v_\theta^{(L)}\cot\theta}{r} + \frac{1}{\rho r\sin\theta}\frac{\partial P^{(L)}}{\partial\phi}$$
$$-a_v\left(\frac{\partial^2 v_\phi^{(L)}}{\partial r^2} + \frac{2}{r}\frac{\partial v_\phi^{(L)}}{\partial r}\right) - a_h\left[\frac{1}{r^2}\frac{\partial}{\partial\theta}\left(\frac{1}{\sin\theta}\frac{\partial}{\partial\theta}\left(v_\phi^{(L)}\sin\theta\right)\right) + \frac{1}{r^2\sin^2\theta}\frac{\partial^2 v_\phi^{(L)}}{\partial\phi^2} + \frac{2\cot\theta}{r^2\sin\theta}\frac{\partial v_\theta^{(L)}}{\partial\phi}\right] = 0, \tag{B.8}$$

and

$$\frac{\partial v_\theta^{(l)}}{\partial t} - 2\Omega v_\phi^{(l)} \cos\theta + \frac{v_\theta}{r}\frac{\partial v_\theta^{(l)}}{\partial \theta} + \frac{v_\phi}{r\sin\theta}\frac{\partial v_\theta^{(l)}}{\partial \phi} - \frac{v_\phi v_\phi^{(l)} \cot\theta}{r} + \frac{1}{\rho r}\frac{\partial P^{(l)}}{\partial \theta}$$
$$-a_v\left(\frac{\partial^2 v_\theta^{(l)}}{\partial r^2} + \frac{2}{r}\frac{\partial v_\theta^{(l)}}{\partial r}\right) - a_h\left[\frac{1}{r^2}\frac{\partial}{\partial\theta}\left(\frac{1}{\sin\theta}\frac{\partial}{\partial\theta}\left(v_\theta^{(l)}\sin\theta\right)\right) + \frac{1}{r^2\sin^2\theta}\frac{\partial^2 v_\theta^{(l)}}{\partial\phi^2} - \frac{2\cot\theta}{r^2\sin\theta}\frac{\partial v_\phi^{(l)}}{\partial\phi}\right] = 0,$$

$$\frac{\partial v_\phi^{(l)}}{\partial t} + 2\Omega v_\theta^{(l)} \cos\theta + \frac{v_\theta}{r}\frac{\partial v_\phi^{(l)}}{\partial \theta} + \frac{v_\phi}{r\sin\theta}\frac{\partial v_\phi^{(l)}}{\partial \phi} + \frac{v_\phi v_\theta^{(l)} \cot\theta}{r} + \frac{1}{\rho r\sin\theta}\frac{\partial P^{(l)}}{\partial \phi}$$
$$-a_v\left(\frac{\partial^2 v_\phi^{(l)}}{\partial r^2} + \frac{2}{r}\frac{\partial v_\phi^{(l)}}{\partial r}\right) - a_h\left[\frac{1}{r^2}\frac{\partial}{\partial\theta}\left(\frac{1}{\sin\theta}\frac{\partial}{\partial\theta}\left(v_\phi^{(l)}\sin\theta\right)\right) + \frac{1}{r^2\sin^2\theta}\frac{\partial^2 v_\phi^{(l)}}{\partial\phi^2} + \frac{2\cot\theta}{r^2\sin\theta}\frac{\partial v_\theta^{(l)}}{\partial\phi}\right] = 0. \quad \text{(B.9)}$$

Let's re-arrange (B.8) first. By introducing the ensemble averaged (resolved) and the unresolved flow scales $v_\theta^{(L)} = \overline{v}_\theta^{(L)} + v_\theta'$, and $v_\phi^{(L)} = \overline{v}_\phi^{(L)} + v_\phi'$ for each velocity component, ensemble averaging, and grouping the unresolved part of the nonlinear Reynolds stress to the right-hand-side of the equations the following gyre-scale equations are obtained:

$$\frac{\partial \bar{v}_\theta^{(L)}}{\partial t} - 2\Omega \bar{v}_\phi^{(L)} \cos\theta + \frac{\bar{v}_\theta^{(L)}}{r}\frac{\partial \bar{v}_\theta^{(L)}}{\partial \theta} + \frac{\bar{v}_\phi^{(L)}}{r\sin\theta}\frac{\partial \bar{v}_\theta^{(L)}}{\partial \phi} - \frac{\bar{v}_\phi^{(L)2} \cot\theta}{r} = -\frac{1}{\rho r}\frac{\partial \overline{P}^{(L)}}{\partial \theta}$$
$$+\left(a_v + \nu_{T_v}\right)\left(\frac{\partial^2 \bar{v}_\theta^{(L)}}{\partial r^2} + \frac{2}{r}\frac{\partial \bar{v}_\theta^{(L)}}{\partial r}\right)$$
$$+\left(a_h + \nu_{T_h}\right)\left[\frac{1}{r^2}\frac{\partial}{\partial\theta}\left(\frac{1}{\sin\theta}\frac{\partial}{\partial\theta}\left(\bar{v}_\theta^{(L)}\sin\theta\right)\right) + \frac{1}{r^2\sin^2\theta}\frac{\partial^2 \bar{v}_\theta^{(L)}}{\partial\phi^2} - \frac{2\cot\theta}{r^2\sin\theta}\frac{\partial \bar{v}_\phi^{(L)}}{\partial\phi}\right],$$

$$\frac{\partial \bar{v}_\phi^{(L)}}{\partial t} + 2\Omega \bar{v}_\theta^{(L)} \cos\theta + \frac{\bar{v}_\theta^{(L)}}{r}\frac{\partial \bar{v}_\phi^{(L)}}{\partial \theta} + \frac{\bar{v}_\phi^{(L)}}{r\sin\theta}\frac{\partial \bar{v}_\phi^{(L)}}{\partial \phi} + \frac{\bar{v}_\phi^{(L)}\bar{v}_\theta^{(L)} \cot\theta}{r} = -\frac{1}{\rho r\sin\theta}\frac{\partial \overline{P}^{(L)}}{\partial \phi} \quad \text{(B.10)}$$
$$+\left(a_v + \nu_{T_v}\right)\left(\frac{\partial^2 \bar{v}_\phi^{(L)}}{\partial r^2} + \frac{2}{r}\frac{\partial \bar{v}_\phi^{(L)}}{\partial r}\right)$$
$$+\left(a_h + \nu_{T_h}\right)\left[\frac{1}{r^2}\frac{\partial}{\partial\theta}\left(\frac{1}{\sin\theta}\frac{\partial}{\partial\theta}\left(\bar{v}_\phi^{(L)}\sin\theta\right)\right) + \frac{1}{r^2\sin^2\theta}\frac{\partial^2 \bar{v}_\phi^{(L)}}{\partial\phi^2} + \frac{2\cot\theta}{r^2\sin\theta}\frac{\partial \bar{v}_\theta^{(L)}}{\partial\phi}\right],$$

where a turbulent diffusion approximation is used

$$\nu_{T_v}\left(\frac{\partial^2 \bar{v}_\theta^{(L)}}{\partial r^2}+\frac{2}{r}\frac{\partial \bar{v}_\theta^{(L)}}{\partial r}\right)+\nu_{T_h}\left[\frac{1}{r^2}\frac{\partial}{\partial\theta}\left(\frac{1}{\sin\theta}\frac{\partial}{\partial\theta}\left(\bar{v}_\theta^{(L)}\sin\theta\right)\right)+\frac{1}{r^2\sin^2\theta}\frac{\partial^2 \bar{v}_\theta^{(L)}}{\partial\phi^2}-\frac{2\cot\theta}{r^2\sin\theta}\frac{\partial \bar{v}_\phi^{(L)}}{\partial\phi}\right]=$$
$$\frac{\bar{v}_\theta^{(L)}}{r}\frac{\partial \bar{v}_\theta^{(L)}}{\partial\theta}+\frac{\bar{v}_\phi^{(L)}}{r\sin\theta}\frac{\partial \bar{v}_\theta^{(L)}}{\partial\phi}-\frac{\bar{v}_\phi^{(L)2}\cot\theta}{r}-\left(\overline{\frac{v_\theta}{r}\frac{\partial v_\theta^{(L)}}{\partial\theta}+\frac{v_\phi}{r\sin\theta}\frac{\partial v_\theta^{(L)}}{\partial\phi}-\frac{v_\phi v_\phi^{(L)}\cot\theta}{r}}\right),$$

$$\nu_{T_v}\left(\frac{\partial^2 \bar{v}_\phi^{(L)}}{\partial r^2}+\frac{2}{r}\frac{\partial \bar{v}_\phi^{(L)}}{\partial r}\right)+\nu_{T_h}\left[\frac{1}{r^2}\frac{\partial}{\partial\theta}\left(\frac{1}{\sin\theta}\frac{\partial}{\partial\theta}\left(\bar{v}_\phi^{(L)}\sin\theta\right)\right)+\frac{1}{r^2\sin^2\theta}\frac{\partial^2 \bar{v}_\phi^{(L)}}{\partial\phi^2}+\frac{2\cot\theta}{r^2\sin\theta}\frac{\partial \bar{v}_\theta^{(L)}}{\partial\phi}\right]=$$
$$\frac{\bar{v}_\theta^{(L)}}{r}\frac{\partial \bar{v}_\phi^{(L)}}{\partial\theta}+\frac{\bar{v}_\phi^{(L)}}{r\sin\theta}\frac{\partial \bar{v}_\phi^{(L)}}{\partial\phi}+\frac{\bar{v}_\phi^{(L)}\bar{v}_\theta^{(L)}\cot\theta}{r}-\left(\overline{\frac{v_\theta}{r}\frac{\partial v_\phi^{(L)}}{\partial\theta}+\frac{v_\phi}{r\sin\theta}\frac{\partial v_\phi^{(L)}}{\partial\phi}+\frac{v_\phi v_\theta^{(L)}\cot\theta}{r}}\right),$$

(B.11)

and the bar stands for ensemble averaging. Here, ν_{T_v} and ν_{T_h} represent vertical and horizontal turbulent viscosity parameters, which correspond to the Smagorinsky approximation of the non-linear Reynolds stress tensor similar to Eqs. (11), (12), (13). Notably, the gyre-scale Eqs. (B.10) are fully decoupled from the jet-scale solution.

The jet-scale equations are rearranged next by introducing the resolved and unresolved components of the jet-scale solution, $v_\theta^{(l)}=\overline{v}_\theta^{(l)}+v_\theta'$, and $v_\phi^{(l)}=\overline{v}_\phi^{(l)}+v_\phi'$ in (B.9), which after ensemble averaging and using Eq. (B.2) becomes:

$$\frac{\partial \bar{v}_\theta^{(l)}}{\partial t}-2\Omega\bar{v}_\phi^{(l)}\cos\theta+\frac{\left(\bar{v}_\theta^{(l)}+\bar{v}_\theta^{(L)}\right)\partial \bar{v}_\theta^{(l)}}{r\partial\theta}+\frac{\left(\bar{v}_\phi^{(l)}+\bar{v}_\phi^{(L)}\right)}{r\sin\theta}\frac{\partial \bar{v}_\theta^{(l)}}{\partial\phi}-\frac{\left(\bar{v}_\phi^{(l)}+\bar{v}_\phi^{(L)}\right)\bar{v}_\phi^{(l)}\cot\theta}{r}=$$
$$-\frac{1}{\rho r}\frac{\partial \overline{P}^{(l)}}{\partial\theta}+\left(a_v+\nu_{T_v}\right)\left(\frac{\partial^2 \bar{v}_\theta^{(l)}}{\partial r^2}+\frac{2}{r}\frac{\partial \bar{v}_\theta^{(l)}}{\partial r}\right)$$
$$+\left(a_h+\nu_{T_h}\right)\left[\frac{1}{r^2}\frac{\partial}{\partial\theta}\left(\frac{1}{\sin\theta}\frac{\partial}{\partial\theta}\left(\bar{v}_\theta^{(l)}\sin\theta\right)\right)+\frac{1}{r^2\sin^2\theta}\frac{\partial^2 \bar{v}_\theta^{(l)}}{\partial\phi^2}-\frac{2\cot\theta}{r^2\sin\theta}\frac{\partial \bar{v}_\phi^{(l)}}{\partial\phi}\right],$$

(B.12)

$$\frac{\partial \bar{v}_\phi^{(l)}}{\partial t}+2\Omega\bar{v}_\theta^{(l)}\cos\theta+\frac{\left(\bar{v}_\theta^{(l)}+\bar{v}_\theta^{(L)}\right)\partial v_\phi^{(l)}}{r\partial\theta}+\frac{\left(\bar{v}_\phi^{(l)}+\bar{v}_\phi^{(L)}\right)}{r\sin\theta}\frac{\partial v_\phi^{(l)}}{\partial\phi}+\frac{\left(\bar{v}_\phi^{(l)}+\bar{v}_\phi^{(L)}\right)v_\theta^{(l)}\cot\theta}{r}=$$
$$-\frac{1}{\rho r\sin\theta}\frac{\partial \overline{P}^{(l)}}{\partial\phi}+\left(a_v+\nu_{T_v}\right)\left(\frac{\partial^2 \bar{v}_\phi^{(l)}}{\partial r^2}+\frac{2}{r}\frac{\partial \bar{v}_\phi^{(l)}}{\partial r}\right)$$
$$+\left(a_h+\nu_{T_h}\right)\left[\frac{1}{r^2}\frac{\partial}{\partial\theta}\left(\frac{1}{\sin\theta}\frac{\partial}{\partial\theta}\left(\bar{v}_\phi^{(l)}\sin\theta\right)\right)+\frac{1}{r^2\sin^2\theta}\frac{\partial^2 \bar{v}_\phi^{(l)}}{\partial\phi^2}+\frac{2\cot\theta}{r^2\sin\theta}\frac{\partial \bar{v}_\theta^{(l)}}{\partial\phi}\right],$$

where the non-linear Reynolds stress is approximated by turbulent diffusion so that

$$
\begin{aligned}
&\nu_{T_v}\left(\frac{\partial^2 \bar{v}_\theta^{(l)}}{\partial r^2}+\frac{2}{r}\frac{\partial \bar{v}_\theta^{(l)}}{\partial r}\right)+\nu_{T_h}\left[\frac{1}{r^2}\frac{\partial}{\partial\theta}\left(\frac{1}{\sin\theta}\frac{\partial}{\partial\theta}\left(\bar{v}_\theta^{(l)}\sin\theta\right)\right)+\frac{1}{r^2\sin^2\theta}\frac{\partial^2 \bar{v}_\theta^{(l)}}{\partial\phi^2}-\frac{2\cot\theta}{r^2\sin\theta}\frac{\partial \bar{v}_\phi^{(l)}}{\partial\phi}\right]=\\
&\frac{\left(\bar{v}_\theta^{(l)}+\bar{v}_\theta^{(L)}\right)}{r}\frac{\partial \bar{v}_\theta^{(l)}}{\partial\theta}+\frac{\left(\bar{v}_\phi^{(l)}+\bar{v}_\phi^{(L)}\right)}{r\sin\theta}\frac{\partial \bar{v}_\theta^{(l)}}{\partial\phi}-\frac{\left(\bar{v}_\phi^{(l)}+\bar{v}_\phi^{(L)}\right)\bar{v}_\phi^{(l)}\cot\theta}{r}\\
&-\left(\overline{\frac{\left(v_\theta^{(l)}+v_\theta^{(L)}\right)}{r}\frac{\partial v_\theta^{(l)}}{\partial\theta}+\frac{\left(v_\phi^{(l)}+v_\phi^{(L)}\right)}{r\sin\theta}\frac{\partial v_\theta^{(l)}}{\partial\phi}-\frac{\left(v_\phi^{(l)}+v_\phi^{(L)}\right)v_\phi^{(l)}\cot\theta}{r}}\right),
\end{aligned}
$$

$$
\begin{aligned}
&\nu_{T_v}\left(\frac{\partial^2 \bar{v}_\phi^{(l)}}{\partial r^2}+\frac{2}{r}\frac{\partial \bar{v}_\phi^{(l)}}{\partial r}\right)+\nu_{T_h}\left[\frac{1}{r^2}\frac{\partial}{\partial\theta}\left(\frac{1}{\sin\theta}\frac{\partial}{\partial\theta}\left(\bar{v}_\phi^{(l)}\sin\theta\right)\right)+\frac{1}{r^2\sin^2\theta}\frac{\partial^2 \bar{v}_\phi^{(l)}}{\partial\phi^2}+\frac{2\cot\theta}{r^2\sin\theta}\frac{\partial \bar{v}_\theta^{(l)}}{\partial\phi}\right]=\\
&\frac{\left(\bar{v}_\theta^{(l)}+\bar{v}_\theta^{(L)}\right)}{r}\frac{\partial v_\phi^{(l)}}{\partial\theta}+\frac{\left(\bar{v}_\phi^{(l)}+\bar{v}_\phi^{(L)}\right)}{r\sin\theta}\frac{\partial v_\phi^{(l)}}{\partial\phi}+\frac{\left(\bar{v}_\phi^{(l)}+\bar{v}_\phi^{(L)}\right)v_\theta^{(l)}\cot\theta}{r}\\
&-\left(\overline{\frac{\left(v_\theta^{(l)}+v_\theta^{(L)}\right)}{r}\frac{\partial v_\phi^{(l)}}{\partial\theta}+\frac{\left(v_\phi^{(l)}+v_\phi^{(L)}\right)}{r\sin\theta}\frac{\partial v_\phi^{(l)}}{\partial\phi}+\frac{\left(v_\phi^{(l)}+v_\phi^{(L)}\right)v_\theta^{(l)}\cot\theta}{r}}\right).
\end{aligned}
\tag{B.13}
$$

The above equations are further rearranged under condition that $\left|v_\theta^{(L)}\right|<<\left|v_\theta^{(l)}\right|,\left|v_\phi^{(L)}\right|<<\left|v_\phi^{(l)}\right|$ to obtain a fully decoupled model in terms of the jet-scale solution component:

$$
\begin{aligned}
&\frac{\partial v_\theta^{(l)}}{\partial t}-2\Omega v_\phi^{(l)}\cos\theta+\frac{v_\theta^{(l)}}{r}\frac{\partial v_\theta^{(l)}}{\partial\theta}+\frac{v_\phi^{(l)}}{r\sin\theta}\frac{\partial v_\theta^{(l)}}{\partial\phi}-\frac{v_\phi^{(l)}v_\phi^{(l)}\cot\theta}{r}+\frac{1}{\rho r}\frac{\partial P^{(l)}}{\partial\theta}\\
&-\left(a_v+\nu_{T_v}\right)\left(\frac{\partial^2 v_\theta^{(l)}}{\partial r^2}+\frac{2}{r}\frac{\partial v_\theta^{(l)}}{\partial r}\right)\\
&-\left(a_h+\nu_{T_h}\right)\left[\frac{1}{r^2}\frac{\partial}{\partial\theta}\left(\frac{1}{\sin\theta}\frac{\partial}{\partial\theta}\left(v_\theta^{(l)}\sin\theta\right)\right)+\frac{1}{r^2\sin^2\theta}\frac{\partial^2 v_\theta^{(l)}}{\partial\phi^2}-\frac{2\cot\theta}{r^2\sin\theta}\frac{\partial v_\phi^{(l)}}{\partial\phi}\right]=0,\\
&\frac{\partial v_\phi^{(l)}}{\partial t}+2\Omega v_\theta^{(l)}\cos\theta+\frac{v_\theta^{(l)}}{r}\frac{\partial v_\phi^{(l)}}{\partial\theta}+\frac{v_\phi^{(l)}}{r\sin\theta}\frac{\partial v_\phi^{(l)}}{\partial\phi}+\frac{v_\phi^{(l)}v_\theta^{(l)}\cot\theta}{r}+\frac{1}{\rho r\sin\theta}\frac{\partial P^{(l)}}{\partial\phi}\\
&-\left(a_v+\nu_{T_v}\right)\left(\frac{\partial^2 v_\phi^{(l)}}{\partial r^2}+\frac{2}{r}\frac{\partial v_\phi^{(l)}}{\partial r}\right)\\
&-\left(a_h+\nu_{T_h}\right)\left[\frac{1}{r^2}\frac{\partial}{\partial\theta}\left(\frac{1}{\sin\theta}\frac{\partial}{\partial\theta}\left(v_\phi^{(l)}\sin\theta\right)\right)+\frac{1}{r^2\sin^2\theta}\frac{\partial^2 v_\phi^{(l)}}{\partial\phi^2}+\frac{2\cot\theta}{r^2\sin\theta}\frac{\partial v_\theta^{(l)}}{\partial\phi}\right]=0,
\end{aligned}
\tag{B.14}
$$

where

$$\nu_{T_v}\left(\frac{\partial^2 \bar{v}_\theta^{(l)}}{\partial r^2}+\frac{2}{r}\frac{\partial \bar{v}_\theta^{(l)}}{\partial r}\right)+\nu_{T_h}\left[\frac{1}{r^2}\frac{\partial}{\partial\theta}\left(\frac{1}{\sin\theta}\frac{\partial}{\partial\theta}\left(\bar{v}_\theta^{(l)}\sin\theta\right)\right)+\frac{1}{r^2\sin^2\theta}\frac{\partial^2 \bar{v}_\theta^{(l)}}{\partial\phi^2}-\frac{2\cot\theta}{r^2\sin\theta}\frac{\partial \bar{v}_\phi^{(l)}}{\partial\phi}\right]=$$
$$\frac{\bar{v}_\theta^{(l)}}{r}\frac{\partial \bar{v}_\theta^{(l)}}{\partial\theta}+\frac{\bar{v}_\phi^{(l)}}{r\sin\theta}\frac{\partial \bar{v}_\theta^{(l)}}{\partial\phi}-\frac{\bar{v}_\phi^{(l)2}\cot\theta}{r}-\left(\overline{\frac{v_\theta^{(l)}}{r}\frac{\partial v_\theta^{(l)}}{\partial\theta}+\frac{v_\phi^{(l)}}{r\sin\theta}\frac{\partial v_\theta^{(l)}}{\partial\phi}-\frac{v_\phi^{(l)}v_\phi^{(l)}\cot\theta}{r}}\right),$$

(B.15)

$$\nu_{T_v}\left(\frac{\partial^2 \bar{v}_\phi^{(l)}}{\partial r^2}+\frac{2}{r}\frac{\partial \bar{v}_\phi^{(l)}}{\partial r}\right)+\nu_{T_h}\left[\frac{1}{r^2}\frac{\partial}{\partial\theta}\left(\frac{1}{\sin\theta}\frac{\partial}{\partial\theta}\left(\bar{v}_\phi^{(l)}\sin\theta\right)\right)+\frac{1}{r^2\sin^2\theta}\frac{\partial^2 \bar{v}_\phi^{(l)}}{\partial\phi^2}+\frac{2\cot\theta}{r^2\sin\theta}\frac{\partial \bar{v}_\theta^{(l)}}{\partial\phi}\right]=$$
$$\frac{\bar{v}_\theta^{(l)}}{r}\frac{\partial \bar{v}_\phi^{(l)}}{\partial\theta}+\frac{\bar{v}_\phi^{(l)}}{r\sin\theta}\frac{\partial \bar{v}_\phi^{(l)}}{\partial\phi}+\frac{\bar{v}_\phi^{(l)}\bar{v}_\theta^{(l)}\cot\theta}{r}-\left(\overline{\frac{v_\theta^{(l)}}{r}\frac{\partial v_\phi^{(l)}}{\partial\theta}+\frac{v_\phi^{(l)}}{r\sin\theta}\frac{\partial v_\phi^{(l)}}{\partial\phi}+\frac{v_\phi^{(l)}v_\theta^{(l)}\cot\theta}{r}}\right).$$

Here the bar stands for ensemble averaging. For approximation of the vertical and horizontal turbulent viscosity ν_{T_v} and ν_{T_h}, the Smagorinsky eddy viscosity model could be used. However, for simplicity of the semi-analytical two-scale model, all scales finer than the small scales l,τ are neglected, that is assuming that the small scales l,τ of the two-scale model represent the most dynamically important scales of the jet flow, $v_\theta^{(l)}\approx\bar{v}_\theta^{(l)}$ and $v_\phi^{(l)}\approx\bar{v}_\phi^{(l)}$ and $\nu_{T_v}=\nu_{T_h}=0$ so that the final jet-scale equations become:

$$\frac{\partial v_\theta^{(l)}}{\partial t}-2\Omega v_\phi^{(l)}\cos\theta+\frac{v_\theta^{(l)}}{r}\frac{\partial v_\theta^{(l)}}{\partial\theta}+\frac{v_\phi^{(l)}}{r\sin\theta}\frac{\partial v_\theta^{(l)}}{\partial\phi}-\frac{v_\phi^{(l)}v_\phi^{(l)}\cot\theta}{r}+\frac{1}{\rho r}\frac{\partial P^{(l)}}{\partial\theta}$$
$$-a_v\left(\frac{\partial^2 v_\theta^{(l)}}{\partial r^2}+\frac{2}{r}\frac{\partial v_\theta^{(l)}}{\partial r}\right)-a_h\left[\frac{1}{r^2}\frac{\partial}{\partial\theta}\left(\frac{1}{\sin\theta}\frac{\partial}{\partial\theta}\left(v_\theta^{(l)}\sin\theta\right)\right)+\frac{1}{r^2\sin^2\theta}\frac{\partial^2 v_\theta^{(l)}}{\partial\phi^2}-\frac{2\cot\theta}{r^2\sin\theta}\frac{\partial v_\phi^{(l)}}{\partial\phi}\right]=0,$$

$$\frac{\partial v_\phi^{(l)}}{\partial t}+2\Omega v_\theta^{(l)}\cos\theta+\frac{v_\theta^{(l)}}{r}\frac{\partial v_\phi^{(l)}}{\partial\theta}+\frac{v_\phi^{(l)}}{r\sin\theta}\frac{\partial v_\phi^{(l)}}{\partial\phi}+\frac{v_\phi^{(l)}v_\theta^{(l)}\cot\theta}{r}+\frac{1}{\rho r\sin\theta}\frac{\partial P^{(l)}}{\partial\phi}$$
$$-a_v\left(\frac{\partial^2 v_\phi^{(l)}}{\partial r^2}+\frac{2}{r}\frac{\partial v_\phi^{(l)}}{\partial r}\right)-a_h\left[\frac{1}{r^2}\frac{\partial}{\partial\theta}\left(\frac{1}{\sin\theta}\frac{\partial}{\partial\theta}\left(v_\phi^{(l)}\sin\theta\right)\right)+\frac{1}{r^2\sin^2\theta}\frac{\partial^2 v_\phi^{(l)}}{\partial\phi^2}+\frac{2\cot\theta}{r^2\sin\theta}\frac{\partial v_\theta^{(l)}}{\partial\phi}\right]=0.$$

(B.16)

The governing gyre-scale (B.10) and jet-scale (B.16) equations of the two-scale model are solved with full-slip conditions in each case:

$$\theta_1<\theta<\theta_2,\phi_1<\phi<\phi_2,$$
$$v_\theta^{(L)}(\theta_1,\phi)=v_\theta^{(L)}(\theta_2,\phi)=v_\phi^{(L)}(\theta,\phi_1)=v_\phi^{(L)}(\theta,\phi_2)=0,\qquad\text{(B.17)}$$

and

$$\theta_c - \frac{l_0}{L_0}\frac{\Delta\theta}{2} < \theta < \theta_c + \frac{l_0}{L_0}\frac{\Delta\theta}{2}, \phi_1 < \phi < \phi_2,$$
$$v_\theta^{(l)}(\theta_c - \frac{l_0}{L_0}\frac{\Delta\theta}{2}, \phi) = v_\theta^{(l)}(\theta_c + \frac{l_0}{L_0}\frac{\Delta\theta}{2}, \phi) = v_\phi^{(l)}(\theta, \phi_1) = v_\phi^{(l)}(\theta, \phi_2) = 0, \quad \text{(B.18)}$$

for the gyre scale and the jet-scale solutions, respectively. The total velocity field is found by superposition in accordance with (B.2).

For solution, velocity Eqs. (B.16) and (B.10), are re-arranged into a single normal vorticity equation for each of the gyre and the jet-scale solution components, respectively:

$$\frac{\partial}{\partial t}\zeta^{\perp(L)} = \frac{2\Omega\sin\theta v_\theta^{(L)}}{r} + I^{\text{conv}}\left(v_\theta^{(L)}, v_\phi^{(L)}\right) + (a_h + \nu_{Th})I^h\left(v_\theta^{(L)}, v_\phi^{(L)}\right) + (a_v + \nu_{Tv})I^v\left(v_\theta^{(L)}, v_\phi^{(L)}\right) + f_w^{(L)}, \quad \text{(B.20)}$$

and

$$\frac{\partial}{\partial t}\zeta^{\perp(l)} = \frac{2\Omega\sin\theta v_\theta^{(l)}}{r} + I^{\text{conv}}\left(v_\theta^{(l)}, v_\phi^{(l)}\right) + a_h I^h\left(v_\theta^{(l)}, v_\phi^{(l)}\right) + a_v I^v\left(v_\theta^{(l)}, v_\phi^{(l)}\right) + f_w^{(l)}, \quad \text{(B.21)}$$

where $\zeta^{\perp(i)}$ is normal vorticity and $I^{\text{conv}}\left(v_\theta^{(i)}, v_\phi^{(i)}\right)$, $I^h\left(v_\theta^{(i)}, v_\phi^{(i)}\right)$, $I^v\left(v_\theta^{(i)}, v_\phi^{(i)}\right)$ and $f_w^{(i)}$ are nonlinear convective terms, horizontal and vertical viscous terms, and wind stress curl, respectively, which are described below

$$\zeta^{\perp(i)} = \frac{1}{r\sin\theta}\left(\frac{\partial}{\partial\theta}\left(\sin\theta v_\phi^{(i)}\right) - \frac{\partial v_\theta^{(i)}}{\partial\phi}\right),$$

$$I^{\mathrm{conv}}\left(v_\theta^{(i)}, v_\phi^{(i)}\right) = \frac{1}{r^2\sin\theta}\left[\frac{\partial v_\theta^{(i)}}{\partial\phi}\frac{\partial v_\theta^{(i)}}{\partial\theta} + v_\theta^{(L)}\frac{\partial^2 v_\theta^{(i)}}{\partial\theta\partial\phi} + \frac{1}{\sin\theta}\frac{\partial v_\phi^{(i)}}{\partial\phi}\frac{\partial v_\theta^{(i)}}{\partial\phi} + \frac{v_\phi^{(i)}}{\sin\theta}\frac{\partial^2 v_\theta^{(i)}}{\partial\phi^2} - v_\phi^{(i)}\frac{\partial^2 v_\phi^{(i)}}{\partial\theta\partial\phi}\right.$$
$$-2v_\phi^{(i)}\cot\theta\frac{\partial v_\phi^{(i)}}{\partial\phi} - \sin\theta\frac{\partial v_\theta^{(i)}}{\partial\theta}\frac{\partial v_\phi^{(i)}}{\partial\theta} - \sin\theta v_\theta^{(i)}\frac{\partial^2 v_\phi^{(i)}}{\partial\theta^2} - \cos\theta v_\phi^{(i)}\frac{\partial v_\theta^{(i)}}{\partial\theta} + \sin\theta v_\phi^{(i)} v_\theta^{(i)}$$
$$\left.-\frac{\partial v_\phi^{(i)}}{\partial\theta}\frac{\partial v_\phi^{(i)}}{\partial\phi} - 2\cos\theta v_\theta^{(i)}\frac{\partial v_\phi^{(i)}}{\partial\theta}\right],$$

$$I^{h}\left(v_\theta^{(i)}, v_\phi^{(i)}\right) = \frac{1}{r^3\sin\theta}\left[-\frac{\partial^2}{\partial\phi\partial\theta}\left(\frac{1}{\sin\theta}\frac{\partial}{\partial\theta}\left(v_\theta^{(i)}\sin\theta\right)\right) + \sin\theta\frac{\partial^2}{\partial\theta^2}\left(\frac{1}{\sin\theta}\frac{\partial}{\partial\theta}\left(v_\phi^{(i)}\sin\theta\right)\right)\right.$$
$$+\cos\theta\frac{\partial}{\partial\theta}\left(\frac{1}{\sin\theta}\frac{\partial}{\partial\theta}\left(v_\phi^{(i)}\sin\theta\right)\right) + \frac{\cot\theta}{\sin\theta}\frac{\partial^2 v_\phi^{(i)}}{\partial\phi^2} + \frac{1}{\sin\theta}\frac{\partial^3 v_\phi^{(i)}}{\partial\theta\partial\phi^2} + 2\cot\theta\frac{\partial^2 v_\theta^{(i)}}{\partial\theta\partial\phi} - \frac{2}{\sin^2\theta}\frac{\partial v_\theta^{(i)}}{\partial\phi}$$
$$\left.-\frac{1}{\sin^2\theta}\frac{\partial^3 v_\theta^{(i)}}{\partial\phi^3}\right],$$

$$I^{v}\left(v_\theta^{(i)}, v_\phi^{(i)}\right) = \frac{1}{r^3\sin\theta}\frac{\partial}{\partial r}\left[r^2\frac{\partial}{\partial r}\left(\frac{\partial}{\partial\theta}\left(\sin\theta v_\phi^{(i)}\right) - \frac{\partial v_\theta^{(i)}}{\partial\phi}\right)\right],$$

$$f_w^{(i)} = \frac{\tau_0^{(i)}}{rH_1}\left[\frac{1}{\sin\theta}\left(\frac{\partial}{\partial\theta}\left(\sin\theta\tau_\phi\right) - \frac{\partial\tau_\theta}{\partial\phi}\right)\right],$$

(B.22)

where indices $i = l, L$ correspond to the jet and the gyre-scale components.

Appendix C: Computational implementation

We prepared an object-oriented package for the fast spectral solution of the two-scale double-gyre problem which is provided here as supplementary material. The codes are written and tested using Microsoft Visual C++ 2010 Express. Armadillo, GNUplot, Boost, BLAS and LAPACK libraries for C++ are necessary to be installed for the package content to work properly.

```
- Header file: Class definition and global declarations
#define global definitions.
Function declarations.
class SpectDG{ Spectral Double-gyre class.
public:
    struct Input{}; Input parameters structure.
    void initialize(), run(), output(string); Solution methods.
    SpectDG(Input input) { initialize(input) }; Class constructor.
private:
    Member methods and parameters declarations. }
- Parameter: User input parameters
#define INPUTS
- Initialize: Class parameters initialization.
- Galerkin Weighting:
void spatialMat() {
    vec coef = quad2d (coefFun, BOUNDS); Galerkin Weights space
integration }
- Run: Calculates the solution
void run() {
    spatialMat(); Spatial matrices calculation.
    mat yout = rksim (odesys, BOUNDS); Runge-Kutta integration }
- Output: Visualization and Data saving.
- Main file: Spectral solution object instantiation
void main() {
    Input input = parameters(); Input parameters structure.
    SpectDG spectDG(input); Spectral solution object.
    spectDG.run(); Run the solution.
    spectDG.output(); Save and plot the results. }
```

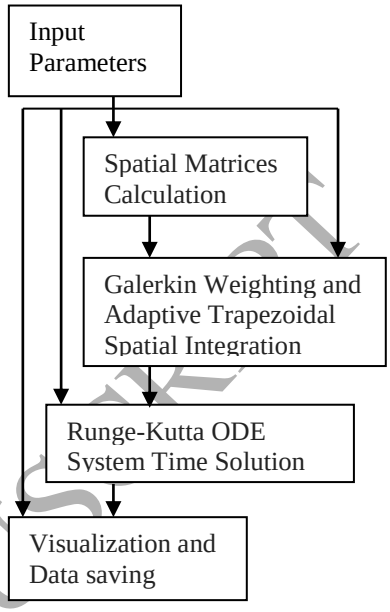

Fig. C1. General algorithm and flowchart of object oriented implementation

As described in Fig. C1, the spectral solution object is defined as an instance of "SpectDG" class. The package consists of the class definition in a header-file (spectdg.h) together with definitions of the class member methods and other functions which are presented in separate files. A function called "parameters" in "parameters.cpp" file stores the user defined input parameters (spectral solution parameters as well as flow parameters adopted from the quasi-geostrophic reference model) in a data structure to be used to instantiate a spectral solution object. The solution is calculated by calling the "run" method and the results are saved and plotted by calling the "output" method. The "run" method uses the class private member methods to solve the problem. These methods are for computing various steps of the spectral solution of double-gyre problem in space as well as its ODE solution in time. First, we formulate different groups of terms such as time derivative, viscous, Coriolis and turbulence terms in their corresponding methods. We then list all the parameters to be integrated in a vector called "coef" in separate files named "coefFun1.cpp" and "coefFun2.cpp". These parameters originate from substituting the assumed double-

summations for velocity components in the introduced groups of terms in the governing equations and multiplying them by the vorticity weighting functions in both jet and gyre-scale solutions.

We integrate the vector "coef", including all the space dependent parts, in the file "spatialMat.cpp" using the adaptive trapezoidal integration method in "quad2d.cpp" to derive final ODE system matrices in the file "odeSys.cpp" as $\dot{\mathbf{Y}}+\mathbf{C}.\mathbf{Y}+\mathbf{N}(\mathbf{Y})=0$ where $\mathbf{Y}=\left[Y_{11}^{(L)}(t)\ \ .\ .\ .\ \ Y_{MN}^{(L)}(t)\ Y_{11}^{(I)}(t)\ \ .\ .\ .\ \ Y_{M'N'}^{(I)}(t)\right]^T$ and $1\le m\le M, 1\le n\le N,$ $1\le m'\le M', 1\le n'\le N'$ and Matrix $\mathbf{C}$ and vector $\mathbf{N}(\mathbf{Y})$ represent all linear and nonlinear terms, respectively. Here, another geophysical dynamics such as the earth's polar motion can easily be coupled to ocean's governing equations by extending the ODE system matrices.

A significant point about this algorithm is the attempt made in it to separate time and space solutions as much as possible, which has considerable effect on the program's run time. We compute all space dependent matrices in one file and integrate them in another and in the end the ODE solver just utilizes constant matrices. This idea is specifically hard to apply when dealing with nonlinear terms which should be updated in each time step and possess complex functionalities in space. The nonlinear terms in the governing equations are the product of two double-summations with time dependent coefficients which are weighted $MN+M'N'$ times by the weighting functions. To avoid these calculations in the time loop, all

```
File- spectdg.h // header file contains global definitions, classes and functions
// include libraries…
// global definitions…
#ifndef GLOBALVARS_H
#define GLOBALVARS_H
 class SpectDG{ // spectral double-gyre class.
 public:
        struct Input{}; // input parameters structure.
        void initialize(); // to initialize the parameters
        void run(); // to run the space and time integrations
        void output(string); // to save and plot the solution result.
        SpectDG(Input input) { initialize(input) }; // class constructor calls initialize method
        ~SpectDG(){}; // class destructor
 private:
        // member methods and parameters declarations. }
// global function declaration.
SpectDG::Input parameters(); // retrieves user input parameters
#endif
File parameter.cpp // return the user input parameters structure
#define INPUTS // user input parameters
SpectDG::Input parameters() {
        SpectDG::Input input={defined parameters…};
        return input; }
File- initialize.cpp // class parameters initialization.
void SpectDG::initialize(SpectDG::Input input) {
        // initialize the solution parameters. }
```

Fig. C2. Pseudo code describing the program outline and all its files.

space dependent parts are previously calculated and saved in a cubic matrix to allow for all the three free indices mentioned. In other words, vector $\mathbf{N}(\mathbf{Y})$, a function of time and space at the same time, is the inner product of a previously calculated space dependent cubic matrix and a time dependent two-dimensional matrix of velocity amplitude products. Finally, in the file "rksim.cpp", we solve the ODE system in time using forth-order Runge-Kutta method. The space and time integration codes are adopted from [37]. The pseudo code describing the whole solution process is given in Fig. C2.

```
File- run.cpp // run the spectral space and time solution
void SpectDG::run(){
        spatialMat(); // spatial matrices calculation.
        mat yout = rksim (&SpectDG::odeSys, y0, ti, tf, dt); // Runge-Kutta integration
        // yout: solution result, y0: initial condition, ti: initial time, tf: final time, dt: time step }

File- output.cpp: // visualization and data saving
void SpectDG::output(string name) {
        yout.save(name, arma_ascii); // save solution in fil name specified by "name"
        yplot(yout); // plot the solution result }

File main.cpp: // to creates and run an instance of the SpectDG class and plot the result
void main() {
        Input input = parameters(); // input parameters structure.
        SpectDG spectDG(input); // spectral solution object.
        spectDG.run(); // run the solution.
        spectDG.output(); // save and plot the results. }

File- spatialMat.cpp // Galerkin weighting: spatial coefficients integration
void SpectDG::spatialMat() {
        // variable initialization…
        vec coef1 = quad2d(coefFun1, t1, t2, f1, f2); // gyre-scale integration
        vec coef2 = quad2d(coefFun2, t1_star, t2_star, f1, f2); // jet-scale integration }

Files- governing_equations_terms.cpp // formulating different groups of terms representing different physics in the
governing equations after substitution of the assumed velocity components
double SpectDG::weight_fun(…){…}
double SpectDG::time_der(…){…}
double SpectDG::visc_ver(…){…}
double SpectDG::visc_hor(…){…}
double SpectDG::eddy_ver(…){…}
double SpectDG::eddy_hor(…){…}
double SpectDG::Coriolis(…){…}

File- coefFun1.cpp // spatial Coefficients for gyre-scale
vec SpectDG::coefFun1(double t, double f){
        // elements of spatial matrices in gyre-scale
        coef(i)=term(i)*weighting function; // term(i) is any of above terms e.g. time derivative, viscosity,..
        return coef; }

File- coefFun2.cpp // spatial coefficients for jet-scale
vec SpectDG::coefFun2(double t, double f){…} // same as above is jet-scale

File- quad2d.cpp // 2D adoptive step trapezoidal integration as in [36]
vec SpectDG::quad2d(…){…}  // second direction integration
vec SpectDG::f11(…){…} // first direction integration
vec SpectDG::f22(…){…} // evaluates the integrand

File- qtrap.cpp // adaptive step trapezoidal integration
vec SpectDG::qtrap(…){…} // adaptive step control as in [36]
vec SpectDG::trapzd(…){…} // trapezoidal integration as in [36]

File- odeSys.cpp // ODE system formulation and time solution
colvec SpectDG::odeSys(double t , colvec Y) {
        // variable initialization…
        // ODE matrices formulation: "A" is the time derivative coefficients matrix and "B" gathers every other term
left in the governing equations
        return solve(A.,B);} // solve for the states' derivatives
File- rksim.cpp // 4th order fixed-step Runge-Kutta as in [36]
mat SpectDG::rksim(colvec (*SpectDG::func)(double, colvec), rowvec y0, double t0, double tf, double th){…}

File- yplot.cpp // plot results
void yplot(mat yout){…} // plot results using GNUplot
```

Fig. C2 (continued). Pseudo code describing the program outline and all its files.

References

[1] N. L. Bindoff, et al., Observations: oceanic climate change and sea level, 2007.

[2] J. Marshall, C. Hill, L. Perelman, A. Adcroft, Hydrostatic, quasi-hydrostatic, and nonhydrostatic ocean modeling, J. Geophys. Res.-Oceans, 102(C3) (1997) 5733-5752.

[3] R. D. Smith, P. R. Gent, Reference manual for the Parallel Ocean Program (POP), ocean component of the Community Climate System Model (CCSM2. 0 and 3.0), Technical Report LA-UR-02-2484, Los Alamos National Laboratory, Los Alamos, NM, 2002.

[4] G. Madec, NEMO ocean engine, 2008.

[5] A. Adcroft, J.M Campin., S. Dutkiewicz, C. Evangelinos, D. Ferreira, G. Forget, B. Fox-Kemper, P. Heimbach, C. Hill, E. Hill, H. Hill, MITgcm user manual, 2014.

[6] A. F. Shchepetkin, J.C. McWilliams, The regional oceanic modeling system (ROMS): a split-explicit, free-surface, topography-following-coordinate oceanic model, Ocean Model., 9(4) (2005) 347-404.

[7] G. Ducrozet, F. Bonnefoy, D. Le Touzé, P. Ferrant, HOS-ocean: Open-source solver for nonlinear waves in open ocean based on High-Order Spectral method. *Comput. Phys. Commun.*, 203 (2016) 245-254.

[8] J. L. Lions, R. Temam, S. Wang, On the equations of the large-scale ocean, Nonlinearity, 5(5) (1992) 1007.

[9] W. H. Munk, On the wind-driven ocean circulation, J. Meteor., 7(2) (1950) 80-93.

[10] W. R. Holland, The role of mesoscale eddies in the general circulation of the ocean-numerical experiments using a wind-driven quasi-geostrophic model, J. Phys. Oceanogr., 8(3) (1978) 363-392.

[11] P. S. Berloff, Random-forcing model of the mesoscale oceanic eddies, J. Fluid Mech., 529 (2005) 71-95.

[12] S. A. Karabasov, P. S. Berloff, V. M. Goloviznin, CABARET in the ocean gyres, Ocean Model., 30(2-3) (2009) 155–168.

[13] I. V. Shevchenko, P. S. Berloff, Multi-layer quasi-geostrophic ocean dynamics in Eddy-resolving regimes, Ocean Model., 94(2015) 1-14.

[14] J. R. Maddison, D. P. Marshall, J. Shipton, On the dynamical influence of ocean eddy potential vorticity fluxes, Ocean Model., 92 (2015) 169-182.

[15] J. Shen, T. T. Medjo, S. Wang, On a wind-driven, double-gyre, quasi-geostrophic ocean model: numerical simulations and structural analysis, J. Comput. Phys. 155(2) (1999) 387-409.

[16] J. Smagorinsky, General circulation experiments with the primitive equations: I. the basic experiment, Mon. Weather Rev., 91(3) (1963) 99-164.

[17] P. A. B. De Sampaio, A Petrov-Galerkin formulation for the incompressible Navier-Stokes equations using equal order interpolation for velocity and pressure, Int. J. Num. Meth. Eng., 31(6) (1991) 1135–1149.

[18] P. A. B. De Sampaio, P. R. M. Lyra, K. Morgan, N. P. Weatherill, Petrov-Galerkin solutions of the incompressible Navier-Stokes equations in primitive variables with adaptive remeshing, Comput. Method Appl. M., 106(1-2) (1993) 143–178.

[19] A. E. Perry, M. S. Chong, A series-expansion study of the Navier–Stokes equations with applications to three-dimensional separation patterns, J. Fluid Mech., 173(1) (2006) 207.

[20] J. S. P. Guerrero, R. M. Cotta, Integral transform solution of developing laminar duct flow in Navier-Stokes formulation, Int. J. Numer. Meth. Fl., 20(11) (1995) 1203–1213.

[21] N. A. Khan, A. Ara, S. A. Ali, A. Mahmood, Analytical Study of Navier-Stokes Equation with Fractional Orders Using He's Homotopy Perturbation and Variational Iteration Methods, Int. J. Nonlin. Sci. Num., 10(2009) (9).

[22] M. M. Rashidi, G. Domairry, New Analytical Solution of the Three-Dimensional Navier–Stokes Equations, Mod. Phys. Lett. B, 23(26) (2009) 3147–3155.

[23] H. Cai, D. Manoussaki, R. Chadwick, Effects of coiling on the micromechanics of the mammalian cochlea. J. R. Soc. Interface, 2(4) (2005) 341–348.

[24] S. Nazarenko, Exact solutions for near-wall turbulence theory, Phys. Lett. A, 264(6) (2000) 444–448.

[25] B. R. Fabijonas, D. D. Holm, Multi-frequency CraikCriminale solutions of the NavierStokes equations, J. Fluid Mech., 506(2004) 207–215.

[26] M. J. Fengler, A Nonlinear Galerkin Scheme Involving Vectorial and Tensorial Spherical Wavelets for Solving the Incompressible Navier-Stokes Equation on the Sphere, PAMM., 5(2005) 457–458.

[27] A. A. Il'In, A. N. Filatov, Unique solvability of Navier-Stokes equations on a two-dimensional sphere, Akademiia Nauk SSSR, 301(1988) 18–22.

[28] C. Cao, M.A. Rammaha, E.S. Titi, The Navier-Stokes equations on the rotating 2-D sphere: Gevrey regularity and asymptotic degrees of freedom, ZAMP, 50(3) (1999) 341–360.

[29] S. Jamal, Solutions of quasi-geostrophic turbulence in multi-layered configurations, Quaestiones Mathematicae, 41(3) (2018) 409-421.

[30] S. E. Naghibi, M. A. Jalali, S. A. Karabasov, M.-R. Alam, Excitation of the Earth's Chandler wobble by a turbulent oceanic double-gyre, Geophys. J. Int., 209(1) (2017) 509-516.

[31] S. Karabasov, D. Nerukh, A. Hoekstra, B. Chopard and P. V. Coveney, Multiscale modelling: approaches and challenges. Philos Trans A Math Phys Eng Sci, 372 (2014) 2021.

[32] S. A. Karabasov, V. M. Goloviznin, Compact accurately boundary-adjusting high-resolution technique for fluid dynamics, J. Comput. Phys., 228(19) (2009) 7426-7451.

[33] S. Butcher, T. King, L. Zalewski, Apocrita - High Performance Computing Cluster for Queen Mary University of London, Queen Mary University of London, Technical Report, 2017.

[34] P. Sagaut, Large eddy simulation for incompressible flows: an introduction, Springer Science & Business Media, 2006.

[35] J. S. Hesthaven, S. Gottlieb, D. Gottlieb, Spectral methods for time-dependent problems, Vol. 21. Cambridge University Press, 2007.

[36] G. K. Vallis, Atmospheric and oceanic fluid dynamics, Cambridge University Press, 2017.

[37] W. H. Press, S. A. Teukolsky, W. T. Vetterling, B. P. Flannery, Numerical Recipes in C, Cambridge University Press, 1988.